This is an *Accepted Manuscript*, which has been through the Royal Society of Chemistry peer review process and has been accepted for publication.

Accepted Manuscripts are published online shortly after acceptance, before technical editing, formatting and proof reading. Using this free service, authors can make their results available to the community, in citable form, before we publish the edited article. We will replace this *Accepted Manuscript* with the edited and formatted *Advance Article* as soon as it is available.

You can find more information about *Accepted Manuscripts* in the **Information for Authors**.

Please note that technical editing may introduce minor changes to the text and/or graphics, which may alter content. The journal's standard **Terms & Conditions** and the **Ethical guidelines** still apply. In no event shall the Royal Society of Chemistry be held responsible for any errors or omissions in this *Accepted Manuscript* or any consequences arising from the use of any information it contains.

The Concept of Mixed Organic Ligands in Metal-Organic Frameworks:
Design, Tuning and Functions

Zheng Yin,[a] Yan-Ling Zhou,[a,b] Ming-Hua Zeng,*[a] Mohamedally Kurmoo[c]

[a] *Key Laboratory for the Chemistry and Molecular Engineering of Medicinal Resources (Ministry of Education of China), School of Chemistry and Pharmaceutical Science, Guangxi Normal University, Guilin 541004, P. R. China.*
[b] *Guangxi Experiment Centre of Science and Technology, Guangxi University, Nanning 530004, P. R. China.*
[c] *Institut de Chimie de Strasbourg, CNRS-UMR7177, Université de Strasbourg, 4 Rue Blaise Pascal, 67008 Strasbourg, France.*

Corresponding authors: zmh@mailbox.gxnu.edu.cn (M.-H. Zeng)

Abstract

The research on metal–organic frameworks (MOFs) has been developing at an extraordinary pace in its two decades of existence, as judged by the exponential growth of novel structures and the constant expansion of its applicability and research scope. A major part of the research and its success are due to the vital role of the concept of mixed organic ligands in the design, tuning and functions. This perspective, therefore, reviews the recent advances in MOFs based on this concept, which is generally based on employing a small polydentate ligand (here labelled as "nodal ligand") to form either clusters, rods or layers which are then connected by a second ditopic linker ligand to form the framework. The structures of the materials can be grouped in the following three categories: layer-spacer (usually known as pillared-layer), rod-spacer, cluster-spacer based MOFs. Depending on the size and geometry of the spacer ligands interpenetration of frameworks are occasionally found. These MOFs show a wide range of properties such as (a) crystal-to-crystal transformations upon solvent modifications, post-synthetic metal exchange or ligand reactions, (b) gas sorption, solvent selectivity and purification, (c) specific catalysis, (d) optical properties including colour change, luminescence, non-linear optic, (e) short- and long range magnetic orderings, metamagnetism and reversible ground-state modifications and (f) drug and iodine carriers with controlled release. In the following, we will highlight the importance of the above concept in the design, tuning, and functions of a selection of existing MOFs having mixed organic ligands and their associated structures and properties. The results obtained so far using this concept look very promising in fine-tuning the pore size and shape for selective adsorption and specificity in catalytic reactions, which appears to be a way to propel the advances in applications and commercialization of MOFs.

1 Introduction

Metal-organic frameworks (MOFs), a subset of coordination chemistry, comprise a wide range of materials where metal centres are connected into infinite arrays by multitopic organic ligands with divergent atoms able to form dative bonds. Due to their infinite nature, they are also classified as coordination polymers. When the ligands are lengthy they often form porous networks that have recently been the principal drive in their development as media for fuel transportation and as catalyst.[1, 2] The chemistry and physics of such porous materials have given rise to a whole gamut of reviews in the past few years highlighting their syntheses, crystal structures and physical properties as well as their wide applications covering gas storage[3], separation[4], catalysis[5], luminescence[6], sensing[7], magnetism[8], and

others.[9] The literature provides also an elegant list of potential applications based on either their structures or their physical properties.

As inorganic-organic hybrid materials, the primary choice of the organic part has been polycarboxylates and polypyridines, and most recently the azolates are increasingly becoming important.[10] Rigid and planar 1,4-benzenedicarboxylate and its progressively longer and modified derivatives were pursued in the synthesis of MOFs and have achieved great success.[11] When assembled with Zn^{II} ions, such ditopic benzene-carboxylate linear ligands led to a series of isoreticular MOFs that are porous with progressive void spaces ranging from 55.8 to 91.1% of the total volume.[12] Benzene poly-carboxylates with three or four carboxylates are also used to prepare MOFs.[13] HKUST-1 constructed from copper ions and trimesate (1,3,5-benzene tricarboxylate) offers an excellent example for the preparation of molecular analogue of zeolites. In a parallel way, multi-N-donors ligands were widely utilized in expanding the scope of MOFs.[14] The combination of metal-unit with a linear bridging ligand of pyrazine and its derivative like 4,4′-bipyridyl, 1,2-bis(4-pyridyl)ethene, *trans*-4,4′-azobis(pyridine), 4,4′-bis(4-pyridylmethoxy)benzene and others can afford diverse structural arrays like 1D chain, 2D (4,4) grid, 3D diamond network based on the coordination geometries of the metal ions.[15] Networked molecular cages with formula of M_xL_y constructed from multi-bipyridyl ligands with kinked donors were also developed.[16] Derivative organic ligands process both carboxylate group and N donors are also well investigated to assemble MOFs.[17] Thus, the chemistry of MOF has been dominated by these ligands.

Scheme 1 Concept of mixed organic ligands MOFs.
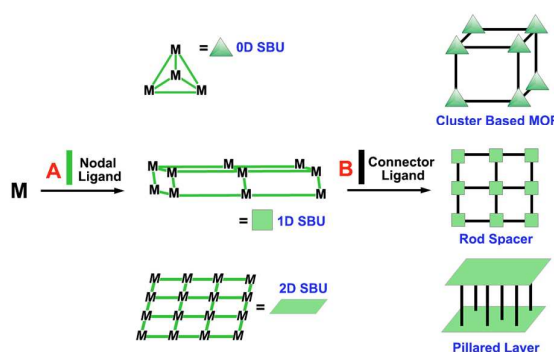
Sometimes, the above organic ligands are simultaneously used to generate the mixed ligands MOFs (Scheme 1).[18] Compared to single ligand MOFs, mixed ligands ones have reached a new level of rational design and construction, which involves the synergetic coordination of different ligands with metals and subsequent networking. When two or more organic ligands are used, they often cooperate with each other to avoid the formation of single ligand MOFs. Numbers of parameters needed to be taken into account in such system, such as solubility of ligands, competition of ligands to coordination with metal ions, thermodynamics and dynamics equilibrium, crystal growth and others. Some quite interesting structural motifs like pillared-layer have proved the importance and success of the mixed ligands strategy.[19] Apparently, the advances made towards mixed ligands MOFs would be helpful for better understanding and extending the synthetic chemistry of MOFs.

Our group has long focused on the coordination chemistry of linear pyridine carboxylate ligands -nicotinate (ina) and its elongated derivatives- that combine the beneficial structural features of benzene carboxylate and poly-pyridine ligands. Using only such linear linker with asymmetric coordination sites, some interesting structures having the 4-connected diamond and higher connected frameworks, or interpenetrated and interdigitated layers have been synthesised.[20] When an additional complementary organic ligands such as a polycarboxylate or a small polydentate chelating ligand like lactate, glycolate,

3-hydroxypicolinate was introduced, we found the one metal node changes to more complex SBUs having 0D polynuclear cluster, 1D chain or rod or 2D layer. Connecting these SBUs by linear linkers like pyridine-carboxylate results in structures of polynuclear cluster-spacer,[21] rod-spacer MOFs,[23] and pillared-layer,[22] respectively. As a result, 1D regular channel, 2D interconnected void, or 3D threading of cages are generated. Subsequently, they show wide applications in selective separation, sensing and especially hosting guest molecules. Moreover, by modifying the ligands the structures also modify the shapes, sizes of the channels and also their windows. Due to high-stability of these structures, PSM of the SBU or the linker can also be applied to modify the structures and functions.[24, 25]

Important as they are, previous reviews seldom evaluate MOFs from a viewpoint of mixed organic ligands because most of them focus on the chemistry of a special ligand family. Du and co-workers presented a selected part according to such thought last year.[26] They summarize a number of MOFs adapting acid–acid, acid-base and base-base mixed ligand strategy and also the influence of solvent, pH condition, metal ions and synthetic route on the assembly. The aim of present review is to highlight the use of the concept of mixed organic ligands, where two or more organic ligands have independent role in the development of different structural topologies, from a range of materials from our laboratory and some selected typical examples from others. Especially we will mainly focus on the critical role of matching mixed ligands of different size, shape, coordination features and the resulting 3D structures of cluster based MOFs, pillared-layer, rod-spacer, special interpenetrated system and also some related pillared-bilayer and interdigitated structures. These compounds not only show interesting structure array and various crystal to crystal transformation but also unique performance in magnetism, iodine enrichment and controlled releasing, heterogeneous catalysis, luminescent sensing and other properties. PSM can also be applied to modify their structures and properties.

Notably, mixed organic ligands MOFs belong to a wide category given that the concept of MOFs has been greatly extended in recent years. Therefore, in this contribution our aim is not to give a list of mixed ligands MOFs. On this account, to better clarify the definition of mixed organic ligands MOFs, examples containing small bridging ligands such as O_2^-, OH^-, NO_3^-, CO_3^{2-}, N_3^-, and SCN^- will not be considered. The first section will focus on pillared-layer mixed ligands MOFs and their magnetic properties, and the flexibility of 2D pillared-bilayer or interdigitated structures. The second section will concern with rod-spacer mixed ligands MOFs, their application in hosting functional guest like iodine, drugs and related host-guest interactions. The third section will give some rare examples of polynuclear cluster based mixed ligands MOFs. The fourth section will concentrate on some structurally interesting interpenetrated mixed ligands MOFs. The selected examples aggregate most of the current research hot spots of MOFs. As the first of its kind, the present review is aimed to highlight the infinite choices of several organic ligands to design MOF from a wider range of parameters to provide tuning of pores and window sizes and shapes and functions.

2 Pillared-layer mixed ligands MOFs

Pillared-layer MOFs are constructed from infinite layers pillared by linear bidentate linkers through dative bonds or supramolecular interactions. Such topology has highly advanced in recent years due to the combined use of bipyridine and polycarboxylate.[27] In this part, we will first discuss a selection of examples of non-interpenetrated 3D pillared-layer mixed ligands MOFs and their magnetic properties, in particular, the solvent effects on the long-range magnetic ordering and in some cases, the metamagnetic behaviour, as well as gate-opening effect, and post-synthetic modification of the frameworks. The second part will highlight some 2D pillared-bilayer and interdigitated structures as well as their dynamic structural transformations including distortion of coordination geometries, rotation of the pillars, slipping of layers or pillared-bilayer.

2.1 3D Pillared-layer mixed ligands MOFs

In a series of our works, flexible polycarboxylate like malate, tricarballylate, D-(+)-camphorate, and succinate or multi-dentate ligand like 3-hydroxypicolinate, pyrazinedicarboxylate, hydroxy-phenyl-acetate were used as the nodal ligands to form layered SBUs. These SBUs are linked by the linear ditopic linker ligands such as ina, pybz, 4,4′-bipyridine to form different pillared-layer structures without interpenetration (Figure 1).
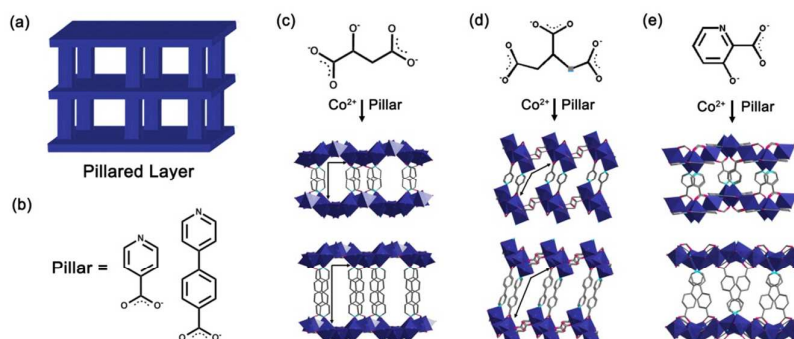
Figure 1 (a) Schematic of a pillared-layer MOF. (b) Pillar ligands (ina and pybz) used for construction. Views of the pillared-layer MOFs using different layer ligands of malate (c), tricarballylate (d) and 3-hydroxypicolinate (e).

The microporous MOF $[Co_2(ma)(ina)]_n \cdot 2nH_2O$ ($1 \cdot 2H_2O$, ma = malate, ina = isonicotinate) featuring a pillared-layered structure was generated by hydrothermal reaction of fumaric acid or maleic acid or maleic anhydride and isonicotinic acid with $Co(NO_3)_2 \cdot 6H_2O$ and a base.[22a] Fumaric acid or maleic acid or maleic anhydride in-situ changed to malate which linked Co^{2+} ions into a $[Co_2(ma)]_n^{n+}$ layer. Within the layer, each ma is coordinated to six Co^{II} ions by eight coordination bonds through two 1,1,3-bridging carboxylate and one μ-alkoxo group (Figure 2). This layer is very rigid and can be simply described by alternative connection of the helices of corner sharing octahedra and trigonal-bipyramids by edge-sharing octahedra running along the a-axis. It represents the first example of an "inorganic" metal-oxygen layer interconnected uniquely by carboxylate and μ-alkoxo groups without the presence of any hydroxyl groups. Such layers are pillared by μ_3-ina ligands in an ABAB mode to form the 3D porous framework with an interlayer distance of 9.09 Å. $1 \cdot 2H_2O$ processes saddle-like channels with window size of 4.5×5.2 Å^2 (Figure 2), corresponding to a 25.8% potential solvent accessible volume, where guest–framework hydrogen bonds anchored the guest water molecules to the layers.
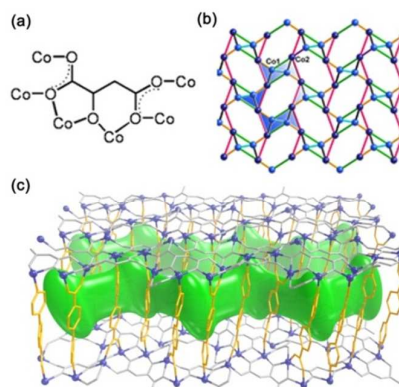
Figure 2 (a) Coordination mode of malate in $1 \cdot 2H_2O$ and $2 \cdot 2H_2O$. (b) View of the layer with Kagome network. (c) View of framework showing the saddle-like 1D channels within $2 \cdot 2H_2O$.

Due to the strong intra- and inter-layer connections, $1 \cdot 2H_2O$ retains its structural integrity up to 340 °C in flowing N_2. The rigid ina-pillared metal-layered structure retains its 3D structural ordering upon guest removal and exchange. Guest-free **1** can also be rehydrated to $1 \cdot 2H_2O$, and transformed to $1 \cdot MeOH$ and $1 \cdot HCONH_2$ by soaking **1** in MeOH and $HCONH_2$ solutions, respectively. The guest-inclusion crystals have been characterized by X-ray single-crystal diffraction, confirming the minimal structural changes of the host framework and modified host–guest and/or guest–guest hydrogen-bonding interactions. The 2D lattice with mixed and multiple exchange-bridges in $1 \cdot 2H_2O$ affords a new geometrical topology different from the kagome lattice and leading to spin frustration (Figure 2). The magnetic behaviours of this family of complexes were reported to originate from the influences of multiple metal sites, intra- and inter-layer exchange, spin–orbit coupling, as well as geometrical frustration. **1**, $1 \cdot MeOH$, $1 \cdot HCONH_2$, and $1 \cdot 2H_2O$ exhibit magnetic ordering at < 2, 3.5, 3.5, and 8 K, respectively, due to the different size of the guest molecules along with the different host–guest interactions, which may slightly modify the magnetic exchange, weaken the spin-frustration within the 2D lattice, and cooperatively enhance the magnetic ordering temperature.

When Hina is changed to the longer 4-(pyridin-4-yl)benzenecarboxylic acid (Hpybz), the corresponding pillared-layer compound $[Co_2(ma)(pybz)]_n \cdot 2nH_2O$ ($2 \cdot 2H_2O$) was obtained.[28] The major part of the structure of $2 \cdot 2H_2O$ is similar to that of $1 \cdot 2H_2O$. Due to the longer pillar, the interlayer distance is increased to 13.2 Å and the solvent accessible volume is increased to 32.3% with larger window size of 8.6×5.2 Å^2 (Figure 2). Dehydrated **2** and guest exchanged $2 \cdot MeOH$, $2 \cdot HCONH_2$, $2 \cdot 1,2\text{-}PrOH$ and $2 \cdot CH_3CN$ were also characterized after single-crystal-to-single-crystal (SC-SC) transformations without major structural deformation due to the highly rigid framework. The antiferromagnetic ordering temperatures T_N of the guest-containing compounds were found to be near 3.6 K and are shifted to 5.0 K after de-solvation. **2** shows saturated CO_2 uptake of 120 cm^3 g^{-1} at 40 bars at room temperature, confirming the permanent micro-porosity of **2**. Notably, the H_2 sorption at 77 K quickly gets saturated at low pressure of 2 bars, while the H_2 absorption is up to 87% of the saturation value at just 0.2 bar. The result confirms the unsaturated coordination metal site exposed in the channels due to the tetragonal pyramid coordination of Co2 ions is beneficial to increase H_2-framework interaction.
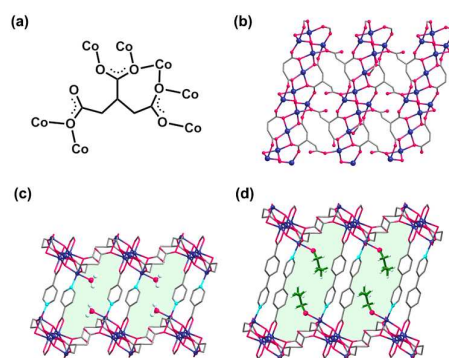
Figure 3 (a) Coordination mode of tricarballylate in $3 \cdot 4H_2O$ and $4 \cdot 2PrOH$. (b) View of the $[Co_5(OH)_2(tca)_2]_n^{n+}$ layer. Views of the 1D channels in $3 \cdot 4H_2O$ (c) and $4 \cdot 2PrOH$ (d) with coordinated H_2O and PrOH hanging in the channels.

In the following, the malate was replaced by tricarballylate and in the presence of Hina or Hpybz to construct magnetic pillared-layer compounds. As a result, the antiferromagnetic pillared-layer MOFs $[Co_5(OH)_2(ina)_2(tca)_2(H_2O)_2]_n \cdot 4nH_2O$ ($3 \cdot 2H_2O$, tac = tricarballylate) and $[Co_5(OH)_2(pybz)_2(tca)_2(C_3H_7OH)_2]_n \cdot 2nH_2O$ ($4 \cdot 2H_2O$) with 1D saddle-like channels have been synthesized and characterized (Figure 3).[29] The layers in $3 \cdot 2H_2O$ and $4 \cdot 2H_2O$ are the same $[Co_5(OH)_2(tca)_2]_n^{n+}$. Different from $1 \cdot 2H_2O$ and $2 \cdot 2H_2O$, the undulated $[Co_5(OH)_2(tca)_2]_n^{n+}$ layer is constructed from

cobalt-oxygen chain and tricarballylate and the layers are pillared by ina or pybz in an inclined way. Notably, coordinated solvent molecules occupy most of the flattened rhombus channels (Figure 3). As a result, there is a guest occupied space of 10.4% for **3**·4H$_2$O and 9.1% for **4**·2H$_2$O. However, the coordinated solvent can be removed by heating without collapse of the framework and create a bigger channel with window size of 5.2 × 4.5 Å^2 and 8.6 × 4.5 Å^2, and increased void volume of 18.0% and 28.9% for [Co$_5$(OH)$_2$(ina)$_2$(tca)$_2$]$_n$ (**3a**) and [Co$_5$(OH)$_2$(pybz)$_2$(tca)$_2$]$_n$ (**4a**) respectively. This also results in stable unsaturated metal site located in the channels. Given that **3a** and **4a** are highly stabile to 380 °C, they have potential application in catalysis.

Inspired by the multiple coordination of the small polycarboxylates the multidentate 3-hydroxypicolinate was introduced to construct the layer. It produced the first structurally authenticated example of polymer featuring homometallic pillared-trilayer structure, [Co$_3$(ina)$_2$(pico)$_2$(H$_2$O)$_2$]$_n$ (**5**, pico = 3-hydroxypicolinate), which was built from mixed pyridyl-carboxylates, isonicotinate and 3-hydroxypicolinate, containing kagome-type trilayers (Figure 4a).[22b] The authors found antiferromagnetic order of **5** and a metamagnetic transition below 3.2 K, and conclude it came from the competing interactions between the antiferromagnetic intralayer couplings of different amplitudes with uncompensated moments versus weak antiferromagnetic interlayer coupling. Such a pico ligand having a hydroxyl group in the pyridyl-type carboxylate provides an additional coordination site and allows the formation of five- and six-membered chelated rings, which can stabilize the resulting solid networks.
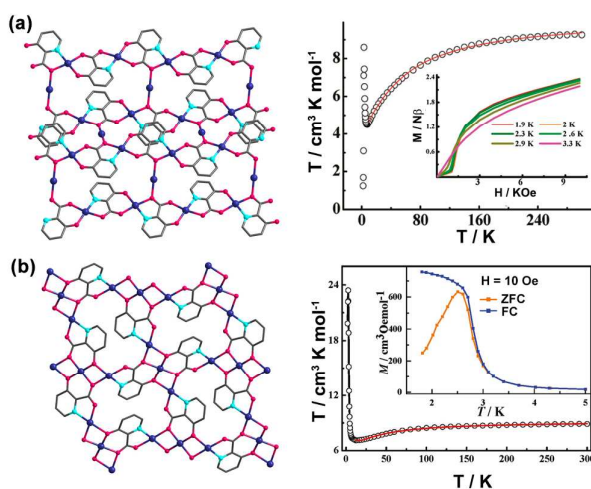
Figure 4 View of layered structures and magnetic properties of **5** (a) and **6** (b).

The short ina pillar was replaced tby the longer pybz with a view to weaken the interlayer antiferromagnetic coupling of [Co$_3$(ina)$_2$(pico)$_2$(H$_2$O)$_2$]$_n$ to get a novel complicated network with ferromagnetic or ferrimagnetic long-range ordering. The magnetic pillared-layer MOF [Co$_3$(pybz)$_2$(pico)$_2$]$_n$ (**6**) was obtained (Figure 4b),[22c] where the coordination mode of pico in **5** and **6** is slightly different, with μ_3-κN,O:κO-μ_2:κO′,O″ and μ_4-κN,O:κO′-μ_2:κO″-μ_2, respectively. As a result, the layer connection of compound **5** and **6** is different even if the content is the same. The [Co$_3$(pico)$_2$]$_n^{2n+}$ layers formed by linear cobalt(II) trimers are cross-pillared by exo-tridentate bridging pybz ligands to form a three-dimensional structure with an unusual uninodal 8-connected body-centred-cubic topology. **6** exhibits ferrimagnetic long-range ordering below 2.6 K, which was suggested to arise from the cooperative magnetic effect of the intra- and inter-trimer arrangements in the 2D magnetic system based on the exchange modes of μ_2-hydroxyl, μ_2-carboxylate oxygen, and 1,1,3-μ_3-carboxylate bridges.
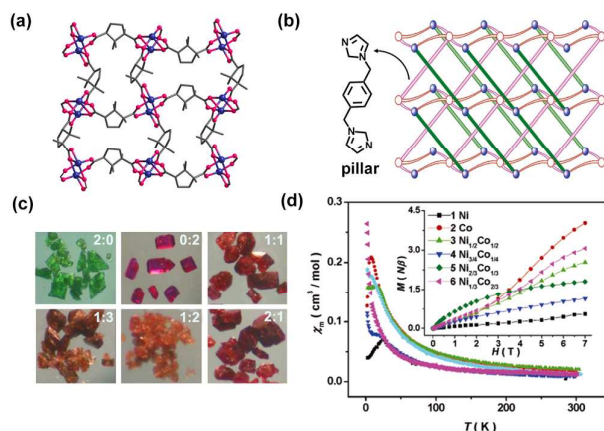
Figure 5 (a) View of the layer connection in **7**. (b) Schematic representation of 1,4-dimb bridging adjacent layers in two different directions of the 3D framework. (c) Colour of crystals of **7** with different ratio of Ni^{2+} and Co^{2+}. (d) χ_M-T plots and field dependence of magnetization (inset) for **7** with different ratio of Co^{2+} and Ni^{2+}.

When the polydentate D-(+)-camphoric acid (H_2ca) is combined with the linear linker 1,4-di-(1-imidazolyl-methyl)-benzene (1,4-dimb), the chiral pillared-layer compounds $[M_xM'_{2-x}(ca)_2(1,4\text{-dimb})]_n$ (**7**, M = Ni^{II}, M' = Co^{II}) were obtained (Figure 5).[30] **7** consists of ca-bridged (4, 4) layers with $[M_2(O_2CR)_4]$ as SBUs that are pillared by 1,4-dimb into the 3D framework. The high-spin octahedral symmetry and the proportions of the mixed metal ions were characterized by UV-vis spectroscopy. The compounds were reported to display antiferromagnetic ordering in the range 7.5-23 K, as well as weak ferromagnetism, spin-flop, and glassy behaviour that result from the randomness of the mixed metal pairs, magnetic anisotropy of the metallic cations, and antisymmetric exchange. The composites should be regarded as molecular alloys of the pure Ni^{II} and Co^{II} compounds. It is reported that the magnetic behaviours of the solid solutions show unambiguously that the organic bridges, bond angles, and bond distances greatly influence the effective interactions and bring about cooperative magnetic behaviour in the chiral 3D frameworks.

When the D-(+)-camphoric acid is combined with Hina, another chiral cluster-based 3D coordination polymer $[Co_2(ca)(ina)_2(H_2O)]_n$ (**8**) was obtained.[31] It contains mixed geometries Co^{II} dimers as subunit, featuring unique corrugated $[Co_2(ina)_2]_n^{2n+}$ 2D layers pillared by the ca ligands. The bridging modes and their intermolecular interactions of the mixed rigid planar ina and flexible bulky ca ligands display an interesting example of shape recognition in packing mode of the 3D frameworks. The authors concluded that bulk antiferromagnetic behaviour mainly arises from the cooperative magnetic effect of the interdimer arrangement in the chiral 3D network based on the nature of the exchange modes of mixed multi-carboxylate bridges within the mixed geometry Co(II) dimer.
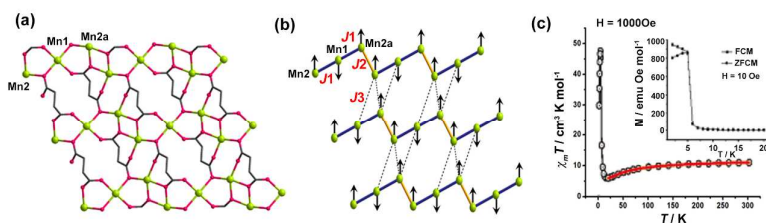
Figure 6 (a) View of the layer structure of **9**. (b) Proposed spin arrangement in the Mn(II) sheet in of the layered structure of **9**. (d) Temperature dependence of $\chi_M T$ *vs* T and FC-ZFC magnetization (inset) for **9**.

Parallel to the above study, succinate was introduced with Hina to construct mixed ligands MOFs. A pillared-layer MOF $[Mn_3(suc)_2(ina)_2]_n$ (**9**, suc = succinate) was synthesized under hydrothermal reaction (Figure 6).[32] Each succinate is coordinated to five octahedra of Mn(II) ions through two similar 1,1,3-μ_3-bridging carboxylate to form edge-sharing trimer. The trimer extends to form a rare example of an "inorganic" metal-oxygen layer interconnected by dicarboxylate ligands without the presence of any hydroxyl groups. Such layers are pillared by μ_3-ina ligands into a 3D framework, with the layers stacking in an AA packing mode and interlayer distance of 9.23 Å. This compound exhibits ferrimagnetic order below 5.0 K, where the ferrimagnetism is present for topological reasons and from the nature of the carboxylate binding modes. The compound was reported to be the first structurally authenticated example of a 3D ferrimagnet, featuring a homometallic topological ferrimagnetic sheet among metal carboxylates.

When hydroxy-phenyl-acetic acid (H_2hypa) reacts with Co^{2+} and 4,4′-bipyridine (4,4'-bpy), the pillared-layer compound $[Co_2(hypa)_2(4,4'-bpy)]$ (**10**) was obtained.[33] **10** has a centro-symmetrical dimeric $Co_2(hypa)_2$ SBU in which the coordination geometry of Co(II) is intermediate between a trigonal–bipyramidal and an square–pyramidal symmetry. The dimer with a very short Co⋯Co distance of 3.021(1) Å is sustained by a pair of μ-alkoxo groups, which is further interconnected by the *syn–anti* carboxylate bridges into neutral 2D layers along [100], with adjacent interdimer Co⋯Co distance of 5.206(1) Å. The 4,4'-bpy ligand acts as pillar to connect the Co(II) ions in the adjacent layers into a 3D pillared-layer structure. Strong antiferromagnetic interaction within the dimer was implied to lead to antiferromagnetic ordering below 15.2 K (T_N) for **10**.
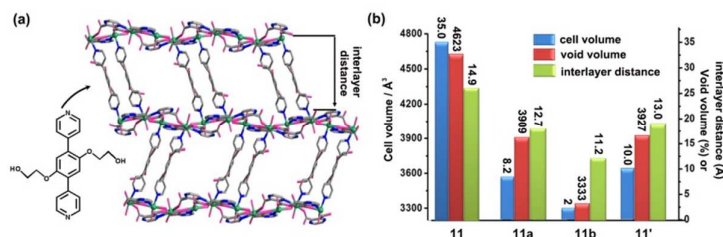
Figure 7 (a) View of the pillared-layer structure of **11**. (b) Comparison of cell volume, void volume and interlayer distance for the four compounds, **11**, **11a**, **11b**, and **11'**.

The above examples mainly focus on the magnetic behaviours of pillared-layer structures for which the character of the layer is relatively more important. In contrast, in some porous pillared-layer structures, the pillars will act as gate to affect the sorption behaviours. Such an example is the 3D pillared-layer compound $\{[Cd_2(pzdc)_2(L1)(H_2O)_2]\cdot 5H_2O\cdot CH_3CH_2OH\}_n$ (**11**, pzdc = 2,3-pyrazinedicarboxylate, L1 = 2,5-bis(2-hydroxyethoxy)-1,4-bis(4-pyridyl)benzene) (Figure 7).[34] Its partially and fully desolvated forms $\{[Cd_2(pzdc)_2(L1)(H_2O)_2]\cdot 3H_2O\cdot CH_3CH_2OH\}_n$ (**11a**) and $[Cd(pzdc)_2L]_n$ (**11b**), respectively and the expanded-intermediate form $\{[Cd_2(pzdc)_2(L1)(H_2O)_2]\cdot 5H_2O\}_n$ (**11'**) were obtained in response to the removal and rebinding of guest molecules in reversible SC-SC manner. The X-ray structure analyses indicated that the 3D host framework is retained during the transformations, and involved mainly rotation of the pillars and slippage of the layers. The structure contracts, the void space decreases and the layers slipped during the removal of the guest molecules (Figure 7). It is noted that the structure of fully desolvated form **11b** has no void volume, but its adsorption isotherm of water at 298 K exhibits three distinct steps coinciding. It also takes up CO_2 (195 K) over N_2 (77 K) and O_2 (77 K). It was believed that these special sorption behaviours come from the highly dynamic structure in which a rotatable pillar bearing ethylene glycol side chains acting as a molecular gate with locking/unlocking interactions triggered by guest inclusion between the side chains.

In contrast to flexible polycarboxylate or multidentate ligand, recently planar and rigid

polycarboxylate like porphyrin has been used as layer ligand.[35] Choe and co-workers conducted a systematic study building a series of porphyrin based pillared-layer frameworks. In a typical example, the porphyrin ligand 5,10,15,20-tetrakis(4-carboxyl)-21H,23H-porphyrin (tcpp) was selected to connect $Zn_2(COO)_4$ paddle-wheel dimers into layers $[Zn_2(Zntcpp)]$.[36] N,N'-di-(4-pyridyl)-1,4,5,8-naphthalenetetracarboxydiimide (dpNI) molecule pillars these layers to form the pillared-layer compound $[Zn_2(Zntcpp)(dpNI)_{1.5}]$ (**12**). Interestingly, when crystals of **12** were introduced into a DEF/EtOH solution containing excess 4,4'-bpy ligands, the long pillars of dpNI were found to be exchanged by the shorter 4,4'-bpy to give the new pillared-layer MOF $[Zn_2(Zntcpp(4,4'-bpy)_{1.5}]$ (**13**).[37] The transformation was 97% accomplished after 2 h. Such post-synthetic ligand exchange reaction is conducted in a SC-SC manner and the c parameters in **12** and **13** are 87.68 and 54.24 Å, respectively, showing the contraction of the c parameter upon replacement of the bridging linker In addition, it was noted that there are two different metal sites (at the centre of the porphyrin and the paddlewheel), which the former is available for axial binding by pillar ligand. Meanwhile, different metal ions coordinated in the porphyrin cores can result in different stacking sequences of 2D metalloporphyrinic layers. As a result, such porphyrin based pillared-layer compounds exhibit various connection schemes.[35]

2.2. 2D thick layer mixed ligands MOFs

Comparing to 3D pillared-layer, when mixed ligands are used, some 2D pillared-bilayers or interdigitated structures can be obtained if the layers cannot extend to an infinite 3D array by the pillar ligands (Figure 8).
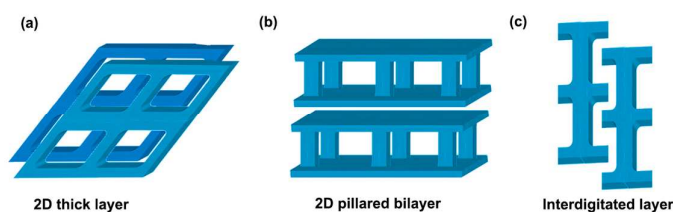
Figure 8 Schematic diagram of 2D layer type MOFs constructed from mixed organic ligands: (a) 2D thick layer with void in the layer. (b) 2D pillared-bilayer with void within and between layers. (c) Interdigitated layers.
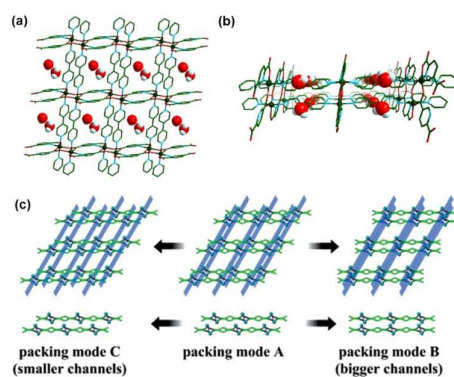
Figure 9 Views of the rectangular-grid framework with void in the layers occupied by H_2O in parallel (a) and vertical directions (b) in **14**·H_2O. Schematic representations of the top and side views of the layer sliding and the contraction or expansion of channels on the removal or addition of guest molecules (c).

In 2004 the 2D thick layer type MOF $[Fe(pydc)(4,4'-bpy)]$·H_2O (**14**·H_2O, pydc = 2,5-pyridinedicarboxylate) was reported.[38] X-Ray single-crystal diffraction of **14**·H_2O reveals that the

Fe(II) ion is located at the centre of a distorted octahedron, being coordinated by three pydc and two 4,4′-bipy ligands (Figure 9). Each pair of Fe(II) ions is bridged by a pair of *syn-syn*-pydc carboxylate groups into a dimeric subunit with an intradimer Fe-Fe distance of 4.430(1) Å. The adjacent dimers are doubly linked by the pydc ligands to form an infinite ribbon, which are further connected through 4,4′-bipy ligands as double bridges (Fe-Fe distance of 11.527(1) Å) into a 2D non-interpenetrating square-grid network with large void space within the layer (atom–atom distance *ca*. 11.5 × 8.8 Å).

Offset stacking of such layers results in small channels perpendicular to the layers, and also gives rise to channels parallel to the layers with solvent accessible volume of 18.4% occupied by lattice water. There exist strong interlayer C–H···O hydrogen bonds between the uncoordinated carboxyl oxygen atoms and pyridyl C–H groups at the edges of adjacent layers. In addition, strong edge-to-face π–π stacking interactions (3.49 Å) between adjacent pydc phenyl groups and 4,4′-bipy pyridyl groups from different layers were present, providing extra interlayer supramolecular forces. $14 \cdot H_2O$ shrinks to the guest-free framework 14_h under heating (up to 160 °C under N_2), or shrinks to another guest-free framework 14_v under vacuum treatment at room temperature while retaining its crystallinity (Figure 9). When the parent single crystals were soaked in MeOH and EtOH, the guest exchanged crystals [Fe(pydc)(4,4′-bipy)]·MeOH ($14 \cdot MeOH$) and [Fe(pydc)(4,4′-bipy)]·EtOH ($14 \cdot EtOH$) were isolated in SC-SC manner. Moreover, the anhydrous 14_v was found to be chemically reactive, taking up ethanol vapour to furnish the solvated crystal structure of an expanded framework $14 \cdot EtOH$. In a mixture of ethanol-DMF or ethanol-benzene, a selective re-solvation process was observed, with only ethanol molecules are inserted into the structure due to the limited free size of the channels in the framework of $14 \cdot H_2O$.
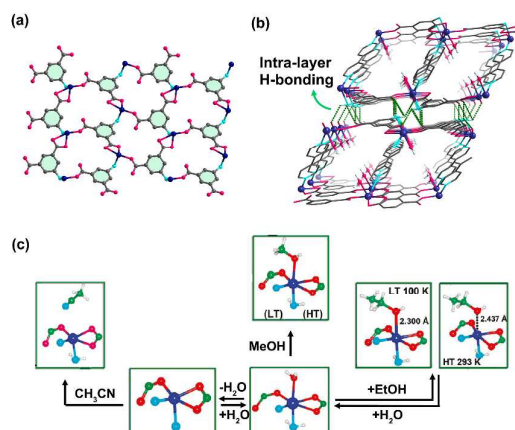
Figure 10 (a) Views of the 2D [Co(5-NH$_2$-bdc)(H$_2$O)]$_n$ layer in $15 \cdot 2H_2O$. (b) Perspective view of the bilayers structure and hydrogen bonding between adjacent layers. (c) Coordination mode changes during SC-SC transformations accompanying apical ligand substitutions.

In another report the 2D pillared-bilayer compound [Co(5-NH$_2$-bdc)(4,4′-bpy)$_{0.5}$(H$_2$O)]$_3$·2H$_2$O ($15 \cdot 2H_2O$, 5-NH$_2$-bdc = 5-aminoisophthalate) was reported.[39] The crystal structure is formed of 2D thin sheets interlinked through bridging 4,4′-bpy ligands into the pillared-bilayer framework (Figure 10). In the neutral and essentially planar infinite 2D [Co(5-NH$_2$-bdc)(H$_2$O)]$_n$ sheet, all terminal water ligands are oriented on the same side of the layer. The bpy acts as pillars to link a pair of such sheets and create 1D channel inside the bilayer which runs along the *b* axis with dimensions of 3.2 × 6.2 Å^2 and water molecules located in these channels. Furthermore, the bilayers are closely packed by fitting the grooves together and interconnected by hydrogen bonding between the amino groups and the carboxylate O atoms. The thickness of the bilayer is 11.31(1) Å and the interspaces between adjacent 2D bilayers are less than 0.5 Å.

Therefore, only the translational motion of guest molecules along the 1D channels inside the pillared-bilayer is permissible. When **15**·2H$_2$O were heated under vacuum to remove the coordinated and guest water molecules, the dehydrated solid [Co(5-NH$_2$-bdc)(bpy)$_{0.5}$] (**15**) was obtained with retention of the crystallinity. Though the framework structure and packing mode are retained, molecular rearrangement involving coordination geometry alteration from an octahedron to a distorted square pyramid of occurs. Accompanying the change of the Co^{II} coordination environment, there is also a colour change from dark-red to purple, a decrease of cell volume, effective windows and interlayer distance. The dehydrated process can be reversed by exposing the dehydrated sample to water vapour with return of the original colour and rearrangement of Co1 to the octahedral coordination geometry.

It is interesting to note that the pillaring 4,4′-bpy ligands are responsible for controlling the overall pillared-bilayer structures, where the probable rotation of pyridyl groups of 4,4′-bpy along the central C-C bond implies that large guest can diffuse out or go inside through the expandable window of the channel. This is confirmed by the sorption behaviours of **15** using large MeOH, EtOH, and benzene molecules. A rapid increase in the amount of adsorbed vapour is shown under low pressure, which indicates the diffusion of adsorbates into the channels. Approximate 1.7 MeOH, 1.2 EtOH, and 0.7 benzene molecules were adsorbed per formula unit at a pressure of 151.1, 70.5, and 113.4 mbar, respectively, despite their diameter (> 3.0 Å) being greater than the narrowest part (1.8 Å) of the rectangular window of **15**. Moreover, adsorption and desorption experiments for EtOH or benzene show the same isotherms (no hysteresis), which indicate that the channel structures are retained through those processes. For MeOH large hysteresis was observed, which suggests that MeOH molecules are confined in each cavity. The porosity of **15** was examined by gas sorption measurements. The adsorption isotherm of N$_2$ at 77 K shows that only surface adsorption has occurred, indicating that nitrogen molecules cannot diffuse into the channels at this temperature. This phenomenon can be attributed to the presence of the narrow pore size of **15**, which does not permit N$_2$ (3.64 Å) to access the channels. Hence, the N$_2$ gas is different from the organic vapour and has no ability to bend or rotate molecular linkages enough to a gate opening at 77 K under low pressure.

Reversible apical ligand substitutions at the Co(II) centre of **15**·2H$_2$O were also studied. When the as-synthesized single crystals were soaked for one day in methanol or ethanol at room temperature, they transformed respectively to [Co(5-NH$_2$-bdc)(4,4′-bpy)$_{0.5}$(MeOH)]·3H$_2$O and [Co(5-NH$_2$-bdc)(4,4′-bpy)$_{0.5}$(EtOH)]·3H$_2$O. Crystallography reveals that MeOH or EtOH has substituted the apical water molecules (Figure 10). During the transformation, no significant change was observed in the unit-cell parameters or the window size of the 1D channel compared to that of the parent host framework. The apical-ligand exchange process can be reversed by immersing [Co(5-NH$_2$-bdc)(4,4′-bpy)$_{0.5}$(EtOH)]·3H$_2$O into water at room temperature. Although alcohols are extremely weak ligands, they are able to substitute coordinated water molecules under circumstances of a highly concentrated organic solvent.

In 2011, a similar 2D pillared-bilayer compound of {[Cd$_4$(azpy)$_2$(pyrdc)$_4$(H$_2$O)$_2$]·9H$_2$O}$_n$ (**16**·9H$_2$O) (azpy = 4,4′-azopyridine, pyrdc = pyridine-2,3-dicarboxylate) was reported.[40] In the asymmetric unit there are two different crystallographically independent hepta-coordinated Cd(II) centres, two pyrdc ligands, and one azpy linker. The pyrdc ligands show two different types of binding modes and connect different Cd(II) centres forming a 2D [Cd$_4$(pyrdc)$_4$]$_n$ corrugated sheet in the *bc* plane (Figure 11). The azpy linker pillars two such 2D sheets along the *a*-axis to form a 2D pillared-bilayer network. The thickness of the bilayer galleries is about ~14.4 Å. The azpy pillars are arranged in a criss-cross and canted fashion that facilitates π-π interaction and results in convex type 1D channels along the crystallographic *c* axis. The 1D channel with window dimension of ~3.5 × 8.8 Å^2 are surrounded by the pyridine moiety of the pyrdc and azpy ligands and are occupied by guest water molecules. The neighbouring bilayers interact to each other by

hydrogen bonding interaction between guest water molecules (O2w and O3w) in the interlayer spaces, the coordinated water molecule (O1w) and O1 oxygen of a carboxylate group of pyrdc, resulting in a 3D supramolecular framework. Therefore the overall framework contains two different spaces: one 1D channel in the intralayer region and the other a 2D space in the interlayer region. The removal of water molecules results in 20.2% of accessible void volume per unit cell. Adsorption experiments of the dehydrated framework **16** for N_2, H_2 at 77 K and CH_4, Ar, O_2 at 195 K show no uptake. However, a single step type I curve was observed for CO_2 (3.3 Å) at 195 K. The diffusion barrier for CO_2 is overcome by specific binding interaction with –N=N– and –COO groups because of its quadrupolar nature. Solvent vapour adsorption studies coupled with PXRD experiments reveal a unique property of the dehydrated solid which indicates that small molecules like MeOH and H_2O are able to diffuse into 2D interlayer spaces along with the 1D channels but not the larger EtOH molecules. This brings out dynamic motion of bilayers during H_2O and MeOH adsorption processes and stepwise profiles ensue.
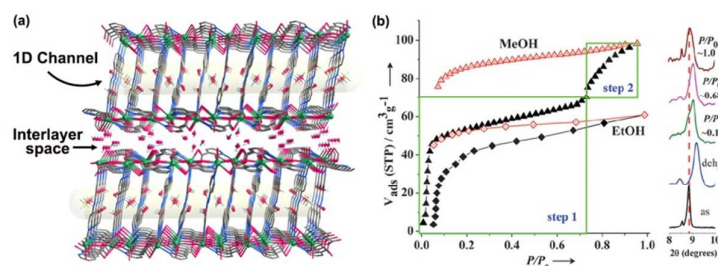
Figure 11 (a) Schematic representations of guest selective accommodation in the 1D channel and the 2D interlayer space in **16**·9H$_2$O. (b) MeOH and EtOH adsorption isotherms for **16** and PXRD pattern of shifting of the 400 peak during MeOH adsorption.

In rare cases, 2D interdigitated layer compound can be synthesized. For example {[Cd(bpndc)(4,4′-bpy)](DMF)(H$_2$O)}$_n$ (**17**) was obtained using mixed ligands benzophenone-4,4′-dicarboxylate (bpndc) and 4,4′-bipyridine (4,4′-bpy).[41] The cadmium are connected by bpndc to produce 1D double-chain {[Cd(bpndc)]}$_n$ running along the *c* axis, which are linked by 4,4′-bpy along the *b* axis to give a 2D sheet motif. The 2D layers are interdigitated to create a 3D assembled framework. The 3D structure of **17** consists of a unidirectional set of non-intersecting linear arrays of cavities (12 × 7 × 4 Å^3) with narrow connecting windows (cross sections of about 2 × 6 Å^2) along [110] or [1-10]. Two water and two DMF molecules occupy the void volume of 29.4%. The solvent molecules can be completely removed by heating to produce the guest-free crystalline phase. It is a flexible framework that shows abrupt changes in its adsorption isotherms with guest dependent gate-opening pressure. The isotherms at 90 K showed a sudden increase at gate-opening pressures P_{go} of O_2, Ar, and N_2 at 3.9, 40.1, and 55.3 kPa, respectively, and attained saturation. It is surprising that the small difference in physical properties between these gas molecules should have such a large effect on P_{go}. On the other hand, desorption isotherms showed adsorption volumes decreasing at lower pressures and large hysteresis loops in the N_2 and Ar isotherms. Adsorption measurements at 77 and 100 K showed that P_{go} increased as the measurement temperature increased. These kinetic analyses indicate that the gate opening process could be associated with the condensation of adsorbate on a crystal surface.

Table 1 Selected examples of 3D pillared-layer or 2D thick layer mixed ligands MOFs.

Nodal Ligand (L)	Pillar Ligand (P)	Formula	Thermal Stability (°C)	Properties	Ref.
		$[Mn_3(L^1)_2(P^1)_2]_n$	-	Ferrimagnetic < 5.0 K	32
		$[Co_2(L^2)(P^1)]_n \cdot 2nH_2O$	340	Guest modified T_N from 2 to 8 K Adsorb H_2O, MeOH, $HCONH_2$	22a
		$[Co_2(L^2)(P^2)]_n \cdot 2nH_2O$	340	Guest modified T_N from 3.6 to 5 K Adsorb H_2O, MeOH, $HCONH_2$, 1,2-PrOH, CH_3CN, CO_2, H_2	28
		$[Co_5(OH)_2(L^3)_2(P^1)_2(H_2O)_2]_n \cdot 4nH_2O$	370	Antiferromagnetic Adsorb Benzene, MeOH	29
		$[Co_5(OH)_2(L^3)_2(P^2)_2(C_3H_7OH)_2]_n \cdot 2nH_2O$	370	Antiferromagnetic Adsorb Benzene, MeOH	29
		$[Co_2(L^4)(P^1)_2(H_2O)]_n$	-	Antiferromagnetic < 7.5 K Chiral framework.	31
		$[M_2(L^4)_2(P^4)]_n$ ($M = Cu^{II}$, $M' = Zn^{II}$)	240	Chiral framework.	44
		$[M_xM'_{2-x}(L^4)_2(P^3)]_n$ ($M = Ni^{II}$, $M' = Co^{II}$)	290-330	Metal doping modified T_N from 7.5 to 23 K Chiral framework.	30
		$[Co_3(L^5)_2(P^1)_2(H_2O)_2]_n$	430	Metamagnetic < 3.2 K	22b
		$[Co_3(L^5)_2(P^2)_2]_n$	460	Ferrimagnetic < 2.6 K	22c
		$[Co_2(L^6)_2(P^3)]$	-	Antiferromagnetic < 15.2 K	33

Nodal Ligand column (left): L^1, L^2, L^3, L^4, L^5, L^6 structures.
Pillar Ligand column: P^1, P^2, P^3, P^4, P^5 structures.

L^7		$[Co(L^7)(P^3)_{0.5}(H_2O)]_3$ $\cdot 2H_2O$	400	Adsorb H_2O, MeOH, EeOH, CH_3CN, Benzene	39
L^8		$\{[Cd(L^8)(P^5)](DMF)(H_2O)\}_n$	-	Selective sorption of CO_2 (195 K) over N_2 (77 K) and O_2 (77 K).	41
L^9	P^6	$[Fe(L^9)(P^3)]\cdot H_2O$	370	Selective sorption of H_2O, MeOH, EeOH over DMF or benzene	38
L^{10}		$\{[Cd_4(L^{10})_2(P^3)_4(H_2O)_2]$ $\cdot 9H_2O\}_n$	240	Adsorb H_2O, MeOH, EeOH Selective sorption of CO_2 (195 K) over N_2 (77 K) and O_2 (77 K).	40
L^{11}	P^7	$[Ni_2(L^{11})(P^8)]\cdot 6H_2O\cdot 3DEF$	300	$S_L = 505$ m^2 g^{-1} (N_2). Selective sorption of CO_2 over CH_4 or N_2.	42a
L^{12}		$[Zn_2(L^{12})(P)]$ $(P = P^3, P^5, P^6)$	300-400	Interpenetration of the framework can be controlled by modify the layer ligand.	42b
	P^8	$[Zn_2(L^{12})(ZnP^7)_{1.5}]$	-	Catalyse acyl-transfer reaction between N-acetylimidazole and 3-pyridylcarbinol with 2420-fold rate enhancement.	43
L^{13}		$[Co_2(CoL^{13})(P^3)_2](NO_3)$	200	-	35b
		$[Zn_2(ZnL^{13})(P^6)_{1.5}]$	-	The P^6 ligand can be replaced by P^3 by PSM	37
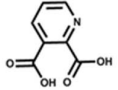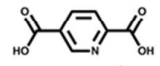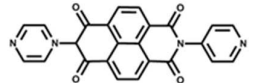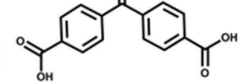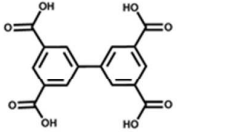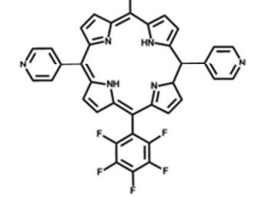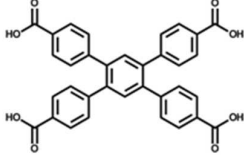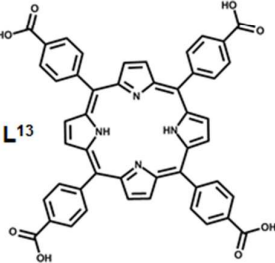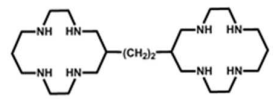
As an important structure category of MOFs, pillared-layer compounds feature a rich variety and interesting functions. As shown in Table 1, mixed ligands strategy is quite beneficial for the construction of pillared-layer structure. From the above examples, flexible polycarboxylate (malate, tricarballylate, *D*-(+)-camphorate, succinate, 3-hydroxypicolinate, hydroxy-phenyl-acetate) can chelate the metal ions or clusters and extend them to layers. Especially, the layer is usually quite compact due to the multiple coordination of the ligand. These layers are pillared by linear ditopic ligands (ina, pybz, and dipyridyl), avoiding the manifestation of interpenetration. In fact, current research has expanded the choice of both the layer ligand and pillar ligand to a widest area.[42] For layer ligand, planar benzene-tetracarboxylate have been used in some reports. Carboxylate or pyridyl group modified porphyrins and metalloporphyrins present an alternative type of layer or pillar ligand to construct functional pillared-layer porphyrinic frameworks.[43] Meanwhile, if chiral layer or pillar ligand was used, chiral framework is generated.[30, 31, 44] The development of both layer and pillar ligand and their countless combinations indicate great abundance of this structure type in the future. Rather than 3D threading void, 2D interconnected or 1D channel was formed using the pillars as walls. The rotation of the pillars control the shape and size of windows of the channels, making pillared-layer structure selectively separate guest molecules. In addition, the above result shows linking together of high magneto-anisotropy systems of lower dimensionality 2D layers into robust 3D lattices provides an important strategy for the generation of porous magnets. The resulting magnetic framework exhibits interesting magnetic behaviour like long-range magnetic ordering or metamagnetism. The guest removal/inclusion/exchange can modify the magnetic properties. Due to strong intra- and inter-layer bonding, most pillared-layer structures possess high stability (Table 1), making them good candidate to be further post-synthetic modified. Subsequently, both the structure and function can be changed in a great extent.

In contrast to the large number of reports of 3D pillared-layer structures, the above 2D pillared-bilayer or interdigitated structures are still accidentally obtained. The limited box space enclosed by ligand within the layers and also the inter-layer void could accommodate guest molecules. Weak interaction such as hydrogen bond or π-π interaction controls the packing, slipping or distortion of the neighbouring layer. This kind of 2D thick layer structures classified between simple thin layers structure and 3D extend structure, and void space, sliding of the layers along with deformation of the layers may be observed simultaneously. Hence, they are quite important for better understanding of current crystalline and solid-state transformations.[45] Especially, the structural motifs of these structures expand or contract reversibly is triggered by removal/recovering/exchange of guest molecules of either organic solvent or gas. This type of unique response behaviour towards small molecules has been studied in separation area and would be a key principle for generation of new materials with exciting guest-responsive properties.

3 Rod-spacer mixed ligands MOFs.

Rod-spacer MOFs are constructed from 1D chains linked by organic linker ligands. Usually, small multidentate ligands are employed to arrange the metal ions into chains that are then linked by bidentate ligands. To successfully construct rod-spacer MOFs, one of the most important factors is the rational design and choice of multidentate ligand of the chain.

Lactic acid was selected as an ideal candidate for constructing the chain due to several advantages: a) it is a flexible ligand, b) it has multiple possible metal binding modes, and c) its molecular coordination chemistry has been well developed. In 2010, a rigid rod-spacer MOF $\{[Zn_3(DL\text{-lac})_2(pybz)_2]\cdot2.5DMF\}_n$ (**18**·2.5DMF) containing mixed ligands, *DL*-lactate (*DL*-lac) and pybz, was obtained (Figure 12).[23] **18**·2.5DMF is built around infinite chains of $\{[Zn_3(DL\text{-lac})_2]^{2+}\}_n$ in which each lactate ligand offers two carboxylate oxygen atoms and the deprotonated hydroxyl oxygen to connect three Zn(II) ions of tetrahedral, trigonal bipyramid and octahedral geometries. These chains were bridged in a square fashion

by a pair of pybz linkers to form the 3D framework. The presence of chains and continuous double walls prevent interpenetration of the framework and resulted in 1D channels (11.2 × 10.2 Å^2). X-ray structure of the de-solvated phase of **18** confirms the framework is quite rigid and the key structural features of **18** are similar to those found for **18**·2.5DMF. There was only a slight structural deformation of the framework due to the lactate anions adopting a monodentate coordination mode linking adjacent Zn^{II} atoms. And consequently the channels adopt a symmetric shape (10.5 × 10.5 Å) corresponding to void volume of 43.5%. Due to the strong intra- and inter-rod connections, **18** show high thermal stability up to 400 °C. This strategy was also successfully applied to construct the Co(II) analogue {[Co$_3$(DL-lac)$_2$(pybz)$_2$]·3DMF}$_n$ (**19**·3DMF).
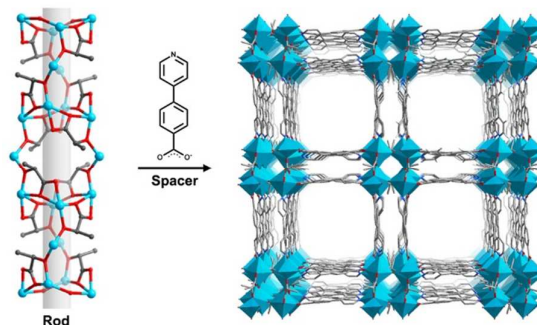
Figure 12 Structure of a [Zn$_3$(*DL*-lac)$_2$]$^{2+}$ chain of the rod-spacer framework of **18**·2.5DMF showing the 1D channels.
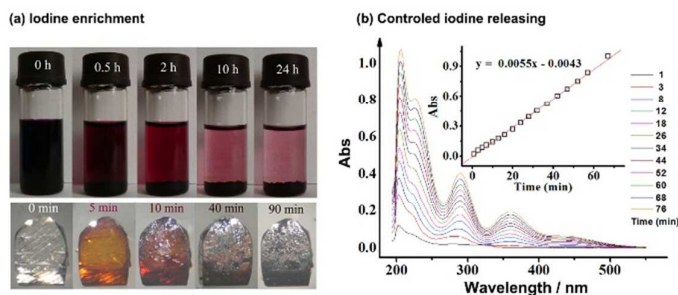
Figure 13 (a) Decolourisation of the solutions and colour change of the single crystal of **18** when soaked in cyclohexane solution of I$_2$. (b) Temporal evolution of UV/vis absorption spectra for the delivery of I$_2$ from **18**·3I$_2$ in EtOH. Inset: fit curves of the controlled delivery of I$_2$ (c[I$_2$] = Kt) in the first 1 h.

The most striking characteristic of this family of compounds is the regular nano-sized 1D channel. Surprisingly, de-solvated crystals of this family show high iodine enrichment when soaked in cyclohexane solution of I$_2$ (Figure 13). The maximum iodine-loading amount is up to 1.01 and 0.9 g/g for **18** and **19**, respectively and gives the formulae **18**·3I$_2$ and **19**·2.7I$_2$. Such iodine uptake is higher than that of zeolite 13X (0.32-0.38 g/g, with 10 Å pore) and activated carbon (~0.84 g/g). IR, Raman, and XRPD data indicates that the resulting iodine inclusion solid retains the host framework crystallinity. Moreover, the I$_2$ delivery in ethanol increases linearly with time, indicating that the I$_2$ release is governed by the host-guest interaction. The release rate of iodine from the iodine-enriched crystal of **18**·3I$_2$ was estimated to be about 170 I$_2$/s within the first 1 h (Figure 13). Once these interactions fade out with increasing I$_2$ extrusion, free diffusion process governed the delivery in the second stage, and a complete I$_2$ release needs more than 11 days to attain the equilibrium state.

More interestingly, iodine loading enhances the electronic conductivities of **18**·3I$_2$ and **19**·2.7I$_2$. Electrical conductivity was measured on single crystals of **18**·3I$_2$ by contacting gold electrodes with gold

paint. The $\sigma_{/\!/}$ and $\sigma_{\perp}$ values were found to be *ca.* 3.42×10^{-3} and 1.65×10^{-4} S/cm, respectively. This is significantly greater ($440\times$) than the generally accepted value ($\sigma = 7.69 \times 10^{-6}$ S/cm) for I_2. An anisotropy factor ($\sigma_{/\!/}$ and $\sigma_{\perp}$) of 21 implied an ordered arrangement mode of I_2 molecules and a preferred conductivity along I_2 chains in the channels. Such enhanced electronic properties are rarely reported in molecular engineered crystals, and this demonstrates the cooperative properties based on host-guest interactions for porous MOF. As a contrast, two-probe electrical conductivity measurement on a powder sample of $\mathbf{19}\cdot2.7I_2$ found the resulting conductivity (σ) is 7×10^{-6} S/cm for $\mathbf{19}\cdot2.7I_2$ which is still higher than the 10^{-6} to 10^{-8} S/m found for the iodine-loaded single crystal of tris(o-phenylenedioxy)cyclotriphosphazene.

The framework constructed from paramagnetic Co^{2+} ions, $\mathbf{19}\cdot3DMF$, is a porous magnet.[23b] Its different guest-loaded forms could be obtained by post-synthetically modification though the exchange of solvents within the voids, desolvation or partial oxidation. In this system, our group characterized the structures and magnetic properties of $\mathbf{19}\cdot6MeOH$, $\mathbf{19}\cdot4.5EtOH$, $\mathbf{19}\cdot3PrOH$, $\mathbf{19}\cdot2C_6H_6$, $\mathbf{19}\cdot2.7I_2$, $\mathbf{19}$, $[Co^{II}_3(lac)_2(pybz)_2(H_2O)_2]\cdot7H_2O$ ($\mathbf{19a}\cdot7H_2O$) and $[Co^{III}Co^{II}_2(lac)_2(pybz)_2(H_2O)_2]\cdot I^-\cdot2H_2O\cdot1.5DMSO$ ($\mathbf{19b}\cdot I^-\cdot2H_2O\cdot1.5DMSO$). The as-prepared $\mathbf{19}\cdot3DMF$ and the solvent exchanged samples and I_2 loaded phase behave as canted antiferromagnets, while upon desolvation $\mathbf{19}$ behaves as a single-chain-magnet. $\mathbf{19}$ is transformed to a ferrimagnet when it is hydrated to $\mathbf{19a}\cdot7H_2O$. By partial oxidation of $\mathbf{19}$ or $\mathbf{19a}\cdot7H_2O$ by I_2 in DMSO/H_2O ferromagnetic $\mathbf{19b}\cdot I^-\cdot2H_2O\cdot1.5DMSO$ is obtained. These transitions from canted antiferromagnetism to single-chain magnetism, to ferrimagnetism, and to ferromagnetism were caused by the PSM of the $\mathbf{19}\cdot3DMF$ which modifies the magnetic exchange interaction between the chains of cobalt ions from being antiferromagnetic through the electron density of the guests in the channel, to being non-existent in the de-solvated $\mathbf{19}$, and finally to ferromagnetic through partial oxidation and incorporation of H_2O and DMSO. This is the first compound to display switching of four magnetic ground states by the modulation of host−guest and Co−O−Co magnetic interactions.
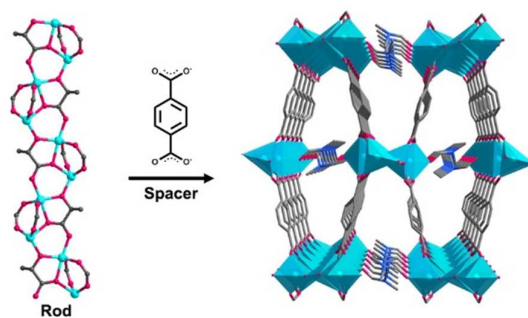
Figure 14 Structure of a $[Zn_2(L\text{-lac})]^{2+}$ chain of the rod-spacer framework $\mathbf{20}\cdot DMF$ with 1D channels.

When chiral lactate was combined with 1,4-benzenedicarboxylate (bdc), the homochiral MOF $[Zn_2(bdc)(L\text{-lac})(DMF)]\cdot(DMF)$ ($\mathbf{20}$) was synthesized by Kim and co-workers (Figure 14).[46] Each lactate dianion connects four Zn^{2+} ions of trigonal-bipyramidal geometry to form 1D chiral chains running along the *a*-axis. These chains act as SBUs, which are linked by benzenedicarboxylate linkers in the other two directions to form a 3D coordination polymer with an open architecture. The pores of roughly 5 Å in diameter are interconnected in three directions. The chiral centres of the *L*-lactate moieties are exposed within the voids and hence the pores in $\mathbf{20}$ have a homochiral environment. Such a 3D homochiral microporous framework has permanent porosity, size and enantioselective guest-sorption properties, as well as remarkable catalytic activity with size- and chemo-selectivity, and high conversion in the oxidation of thioethers to sulfoxides.
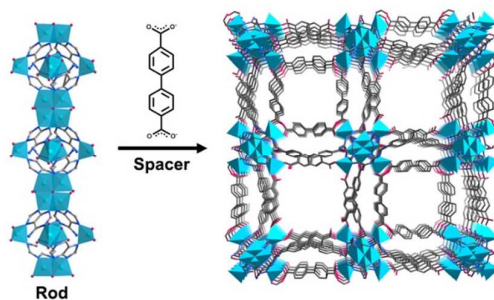
Figure 15 Structure of a $[Zn_8(ad)_4O]^{10+}$ column of the rod-spacer framework **21** with 1D channels.

Multidentate adenine ligand was also used to construct rod-spacer MOF. The reaction of biphenyldicarboxylic acid with adenine and zinc acetate dihydrate in DMF yielded the anionic MOF $Zn_8(ad)_4(bdc)_6O \cdot 2Me_2NH_2 \cdot 8DMF \cdot 11H_2O$ (**21**, Bio-MOF-1, ad = adeninate).[47] It is a permanently porous MOF with infinite zinc-adeninate columnar SBUs that are connected along [100] and [010] by bdc linkers (Figure 15). The SBU columns are composed of apex-sharing zinc-adeninate octahedral cages. Each cage consists of four adeninates that occupy alternating faces of the octahedron and eight Zn^{2+} tetrahedra, four at the corners of the equatorial plane of each cage and two at each apical position. The zinc-adeninate columns are bridged by bdc. This connectivity pattern results in large channels that run along the *c* axis. The anionic nature of **21** is used to store cationic drug procainamide HCl through cation exchange with the $Me_2NH_2^+$, where the maximum loading is 0.22 g drug per gram material after 15 days. More interestingly, steady procainamide release was observed over the course of 20 h in 0.1 MPBS buffer, and complete release was realized after 72 h. This is the first example of cation-triggered drug release from a MOF and also the first demonstration of a potential biomedical application for an MOF constructed with biomolecule building blocks. They further show that the pore size of Bio-MOF-1 can be modified post-synthetically via cation-exchange experiments and that such modifications can be used to systematically tune the CO_2 adsorption capacity of this material.[48] **21** can also incorporate lanthanide cations and the negative framework can protect and sensitizes visible and NIR-emitting lanthanides in water.[49]

From the above examples, we can see that 1D rod-spacer connection usually results in rigid framework and hence high thermal stability. As a result, 1D regular nano-size channel with high void volume can be obtained following heating or vacuuming the solvent out, while retention of the crystallinity. The 1D channel is a good host to capture molecules such as iodine, drugs and others. As the confined guests can just leave form the two opposite windows of the channel, the releasing rate can be controlled by the guest-framework interaction as well as the window size of the channel. Such feature endows rod-spacer MOFs great potential in biomedicine especially drug carrier.[50] In such regular channels, the guest molecules may regularly arrange in the channel due to host-guest interaction and the shape, size, space limitation of the channels. Therefore the framework-guest cooperative properties such as increased conductivity, non-linear optic, and sensitization of lanthanide cation can be anticipated. From another point of view, rod-spacer MOF is good candidate for porous magnet when paramagnetic metal ions are used. The 1D magnetic chain within rod-spacer MOF would be good model of single-chain magnet if long inter-chain linkers were employed to reduce inter-chain magnetic super-exchange. Modulation of T_C, T_N, magnetic hysteresis can be obtained due to the removal/inclusion/exchange of guest molecules. More interesting, when the framework structure is modified in a post-synthetic way, even the change of ground state is feasible. It is believed that magnetic MOFs with rod-spacer feature to be a typical model to investigate switching behaviour and also a good candidate of multifunctional materials. However there are just few examples of such structure type till now. It is necessary to develop synthesis strategy for rod-spacer MOF so as to achieve above function. Inspired by the above successful examples, mixed ligand combination of a small multidentate ligand with linear ditopic linker would be a promising choice.

4 Cluster based mixed ligands MOFs.

Metal cluster based MOFs are constructed by linking polynuclear clusters SBU by organic linkers. Some high-symmetry metal-carboxylate clusters were frequently found as SBUs, for example $Cu_2(COO)_4$ in HKUST-1, $Zn_4(\mu_4\text{-}O)(COO)_6$ in MOF-5, and $Zr_6O_4(OH)_4(COO)_{12}$ in UiO-66. Comparing to these cluster-based MOFs constructed from single organic ligand, appropriate collocation of two different linear ligands may also result in some complex cluster based MOFs.[51] For example, Yaghi *et al.* reported a hierarchical structure $[NH_2(CH_3)_2{}^+]_8[(Fe_3O)_4(SO_4)_{12}(bdc)_6(bpe)_6{}^-]_8\cdot13H_2O\cdot8DMF$(**22**, MOF-500, bpe = *cis*-1,2-bis-4-pyridylethane).[52] In this compound, bdc links the $\{(Fe_3O)(CO_2)_3(SO_4)_3\}$ clusters to form tetrahedral molecular building blocks of $[(Fe_3O)_4(SO_4)_{12}(bdc)_6(py)_{12}]^{8-}$, which are then linked by bpe with an 70.5° angle necessary to covalently link the iron trimers. De-solvated **22** is highly porous with void volume of 78.5% and a BET surface area of 2274 m^2 g^{-1}. Subsequently, Zhou *et al.* reported a metal-organic polyhedra $[(Cu_2)_9(9H\text{-}3,6\text{-}cdc)_6(pddb)_{12}(dma)_6(H_2O)_{12}]\cdot x$S (**23**, S = non-coordinated solvent) constructed from mixed ligands 9H-carbazole-3,6-dicar-boxylate (9H-3,6-cdc) and 4,4′-pyridine-2,6-diyldibenzoate (pddb).[53] The former has a bend angle of about 90°, the latter of 120°. The two bent ditopic ligands link paddle-wheel Cu2 units to form the hendecahedral cage compound with an odd number (eleven) of faces and an odd number (nine) of vertices. Gas sorption studies of evacuated sample of **23** indicate a microporous material with a Langmuir surface area of 372 m^2 g^{-1}.
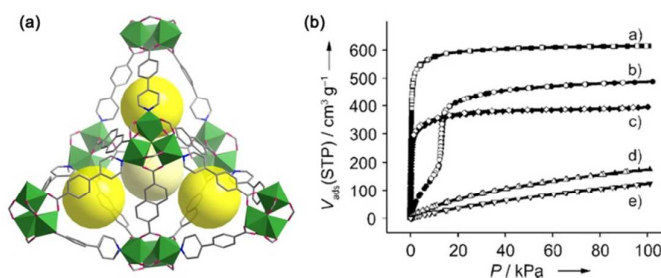
Figure 16 (a) Perspective views of the tetrahedral building units with void cage within the framework. (b) Gas sorption isotherms of desolvated **24**: a) N_2 at 77 K; b) CO_2 at 195 K; c) N_2 at 77 K (partially degassed at 80 °C); d) H_2 at 77 K; e) CH_4 at 195 K.

Chen's group synthesised a highly connected porous mixed-valence MOFs, $[Ni^{II}_2Ni^{III}(\mu_3\text{-}OH)(pybz)_3(ndc)_{1.5}]\cdot9.5DMA\cdot8.5H_2O$ (**24**, ndc = naphthalene-2,6-dicarboxylate) with an unusual channel structure.[54] In this compound, the C_3-symmetric planar $Ni_3(\mu_3\text{-}OH)$ cluster is encapsulated by six carboxylate groups (three from pybz and three from ndc) and three pyridyl groups of pybz to form a tricapped trigonal prismatic $[Ni_3(\mu_3\text{-}OH)(COO)_6]$ cluster (Figure 16). Three ndc and six pybz units connect this SBU into an unprecedented uninodal nine-connected **ncb** net. This 3D framework contains tetrahedral and trigonal-pyramidal cages in the ratio of 1:4. Four SBUs and six ndc units enclose the tetrahedral cage having an internal free diameter of *ca.* 9.3 Å and window diameter of *ca.* 4.7 Å. Four SBUs, three ndc, and three pba units generate the trigonal-pyramidal cage with internal free diameter of *ca.* 8.6 Å. A face of the trigonal-pyramidal cage is also one for the tetrahedral cage, while the other three faces have window diameters of *ca.* 4.2 Å. Therefore, the overall channel system consists of three types of cavities that are connected through three types of small passages, resulting in a unique hierarchical channel-cavity biporous system. The CO_2 sorption of desolvated **24** at 195 K exhibits a two-step behaviour (Figure 16). The saturation sorption amounts of the two steps were estimated to be 352 and 510 cm^3 g^{-1}, respectively, which are a satisfactory match to the calculated pore volumes of the NbO channel (47.3%) and the whole channel system (68.5%). This finding implies that at low P/P_0 the adsorption should mainly occur in the NbO channel, and the triakis tetrahedra cavities are only available at relatively high P/P_0. Consequently, the

apparent Langmuir surface area of the NbO channel and the whole pore can be estimated as 2044 and 2957 $m^2 g^{-1}$, respectively, which illustrates the high porosity of **24**.

Later, the authors investigate the influence of the linker lengths and length ratios of two ligands on the synthesis/construction and framework stabilities by geometry analysis. A systematic approach with 5×5 ligand combinations produced 13 highly porous isoreticular frameworks, which show adjustment of pore volumes (0.49–2.04 $cm^3 g^{-1}$), sizes (7.8–13.0 Å; 5.2–12.0 Å; 7.4–17.4 Å), and anisotropic modulation of the pore shapes.[55] Adapting similar combination of the above mixed ligands and 9-connected **ncb** net, replacing the neutral $[Ni_3(\mu_3\text{-}OH)(COO)_6]$ cluster by positive $[In_3O(COO)_6]^+$ cluster resulted in a family of MOFs with positively charged framework and tuneable pore size.[56] These MOFs can be used to perform selective ion-exchange of organic dyes within $\sim$100Da $<$ Mw$<$ $\sim$1,000Da range. The ion-exchange processes of organic dyes in these MOFs have been demonstrated highly selective based on the basis of charge and size of organic dyes.

To obtain polynuclear cluster based MOF, one perfect synthetic strategy is using small multidentate ligand to pre-assemble the polynuclear SBU, and then linked them by linear linkers. Following such thought, Zhu and co-workers have successfully synthesized the large pore open-framework $[Cd_{11}(\mu_4\text{-}HCOO)_6(bdc)_9]\cdot$9DMF$\cdot$6H$_2$O (**25**), which contains a large Cd(II)–carboxylate cluster SBU and a rare **bcu** topology, by rationally utilizing a flexible organic acid (HCOOH) as a strong bridging ligand.[57] Desolvated **25** possesses pore volume of 0.35 $cm^3 g^{-1}$ and shows good sorption for H$_2$O, CH$_3$OH, C$_2$H$_5$OH and displays optoelectronic properties.
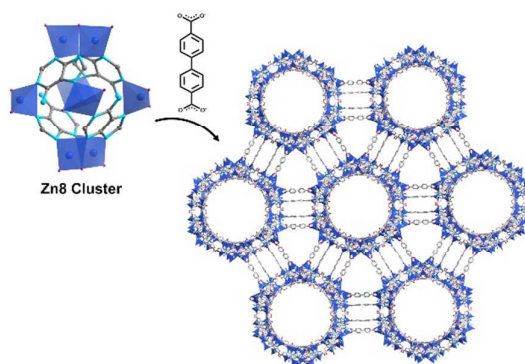
Figure 17 (a) Schematic representation of the construction Zn8 cluster of the 3D framework with large meso-size channels in **26**.

Adeninate was also used to construct polynuclear cluster based MOF $[Me_2NH_2]_4[Zn_8O_2$ (ad)$_4$(bdc)$_6]\cdot$49DMF$\cdot$31H$_2$O (**26**, Bio-MOF-100), which exhibits exclusively meso-sized void (Figure 17).[58] Each cluster consists of eight Zn^{2+} cations interconnected by four adeninates and two μ-oxo groups; monodentate bdc's occupy the remaining coordination sites on each tetrahedral Zn^{2+}. The size of the Zn8 cluster necessitates that three carboxylates coordinate to each open face, resulting in a total of 12 bdc's per unit. The Zn8 cluster measures 14.2 Å from top to bottom and 14.3 Å across its diameter, which is significantly larger than the basic Zn$_4(\mu_4\text{-}O)(COO)_6$ cluster of MOF-5. Twelve bdc linkers connect each cage to four neighbouring clusters. Hence, each Zn-octanuclear connects to neighbouring units with three linkers instead of one; an aspect that may significantly increase the structural robustness of a framework. This connectivity is repeated periodically throughout the extended three-dimensional framework, generating large cavities within the structure and solvent channels measuring $\sim$28 Å in diameter that run along [110], [101] and [011. It is the first MOF material that exclusively exhibits mesopores. As a result, desolvated **26** exhibits a high surface area (4,300 $m^2 g^{-1}$), one of the lowest crystal densities (0.302 g cm^3)

and the largest MOFs pore volume reported to date (4.3 cm^3 g^{-1}). A stepwise post-synthetic ligand exchange strategy is utilized to prepare a series of isoreticular analogues.[59] In situ ligand exchange with progressively longer dicarboxylate linkers of azobenzene-4,4′-dicarboxylate (abdc) and 2′-amino-1,1′:4,1′-terphenyl-4,4″-dicarboxylate (NH$_2$-tpdc) is performed on single crystalline starting materials to synthesize products with progressively larger mesoporous cavities. The new members of this series of materials, Bio-MOFs-100~103, exhibit permanent mesoporosity and pore sizes ranging from ~2.1-2.9 nm and surface area ranging from 2704 to 4410 m^2/g.

Given that the difference of coordination chemistry between different ligands, step by step crystal-engineering strategy can be applied to generate mixed ligands MOFs. Wang and co-workers synthesised three MOFs of [Zn$_5$(btz)$_6$(bdc)$_2$(H$_2$O)$_2$]·7DMA (**27**, btz = benzotriazolate), [Zn$_5$(btz)$_6$(NH$_2$bdc)$_2$(H$_2$O)$_2$]·7DMA (**28**, NH$_2$bdc = amino-1,4-benzenedicarboxylate), and [Zn$_5$(btz)$_6$(bpdc)$_2$(H$_2$O)$_2$]$_{1.5}$·10DMA (**29**, bpdc = 4,4′-biphenyldicarboxylate).[60] In their work, benzotriazolate reaction with Zn(II) ions to generate the stable pentanuclear clusters [Zn$_5$(btz)$_6$(NO$_3$)$_4$(H$_2$O)] (**30**), which can act as initial reaction precursor. The pentanuclear cluster has a tetrahedral structure, where four Zn^{2+} are at the vertices of the tetrahedron with the fifth Zn^{2+} at the centre. Each Zn^{2+} at the apical positions bears a chelating nitrate group. These coordinated nitrate groups could be fully substituted by linear carboxylate ligands. As a result, four-connected diamondoid framework of **28-30** with different interpenetration was obtained.

Zaworotko's group reported another two-step synthetic approach to synthesise cluster based MOFs. Hina reacts with Cr(III) ions resulted in a trigonal prismatic primary molecular building block of [Cr$_3$(μ_3-O)(ina)$_6$] (**31**) in the first step.[61] In the second step, by introduce triangular carboxylate ligands and metal salt under solvothermal reaction, the precursor is dissolved and coordinated to metal cations through its six dangled pyridyl moieties. They successfully synthesized three trinodal (3,4,6)-connected *asc* networks [Zn$_3$(L)$_2${Cr$_3$O(ina)$_6$(H$_2$O)$_2$(OH)}]·*x*DMF (**32**, L = btc = 1,3,5-benzenetricarboxylate; **33**, L = btb = 1,3,5-tris(4-carboxyphenyl)benzene; **34**, L = btctb = 4,4′,4″-[1,3,5-benzenetriyltris (carbonylimino)]trisbenzate). Solvent molecules also represent an opportunity for fine-tuning the pore walls. When heating **31** in pyridine at 105 °C for 24 h, the terminal water ligands of Cr^{III} were replaced by pyridine (py) in a SC-SC process with retention framework, and gives [Zn$_3$(btc)$_2${Cr$_3$O(ina)$_6$(py)$_3$}] (**32a**).

We can conclude that mixed ligands strategy is efficient to construct frameworks with polynuclear cluster building blocks. Without interpenetration, these cluster-based frameworks also result in high void volume and perforated channels. Using step-by-step synthetic approach by first designing precursor clusters with unsaturated coordination sites it is helpful for the construction of cluster based mixed ligands MOFs. The polynuclear cluster is a good precursor to produce stable open metal site, which is urgently needed for study of gas sorption and catalysis. In addition, systematic modulations of pore sizes, shapes of void as well as positively or negatively charged frameworks are feasible by controlling the combination of mixed ligands and also the choice of cluster building blocks. This kind of MOFs provides a unique platform for systematically studying the correlation of structure-property and developing new functional MOFs materials with improved properties.

5 Interpenetrated mixed ligands MOFs.

Interpenetration is an intriguing phenomenon with significant impacts on the structure, porous nature, and functional applications of MOFs. Usually, two or more similar networks are generated from the same combination of ligand and metal ions or clusters. The resulting interpenetrated MOFs vary only in the degree of interpenetration. However, when mixed ligands were used, the difference of coordination chemistry between the ligands may result in different networks.[62] Interpenetration of these different networks enriches the types of structurally interpenetrated systems.

In 2005, the 3D MOF $[Co_4(pico)_4(4,4'-bpy)_3(H_2O)_2]_n \cdot 2nH_2O$ (**35**) consisting of two different interpenetrating 2D neutral polymers was reported (Figure 18).[63] There are four octahedra of Co^{II} in the asymmetric unit of **35**. The pico and 4,4′-bpy ligands link Co1 and Co2 to form A-type sheets $Co_2(pico)_2(4,4'-bpy)(H_2O)_2]_n$ having Co···Co distance of 11.220(2) Å. In this sheet, the pair of pyridyl groups in each 4,4′-bpy ligand is significantly twisted with a dihedral angle of about 168°. The curved conformation of the 4,4′-bpy ligands in the corrugated sheet leads to the existence of two kinds of meshes (atom to atom distance ca. 11.2×7.3 Å^2 and 11.2×3.5 Å^2). Another net of B-type constitutes $[Co_2(pico)_2(4,4'-bpy)_2]_n$, constructed from the ligands and Co3 and Co4. It is a square net with a uniform mesh size (atom to atom distance *ca.* 11.5×11.6 Å^2) different from that in the A-type sheets. Interestingly, the two types of sheets are interpenetrated in a parallel/diagonal inclined fashion with the bigger windows of the A-type nets enclosing the 4,4′-bpy rods of the B-type nets. In addition the windows of the B-type nets contain the nodes of the A-type nets in a 1:1 ratio. This leads to a unique compact 3D network where hydrogen-bonding interactions are present between the sheets. Strong edge-to-face aromatic interactions of 3.56 Å also exist between adjacent 4,4′-bpy groups of different sheets.
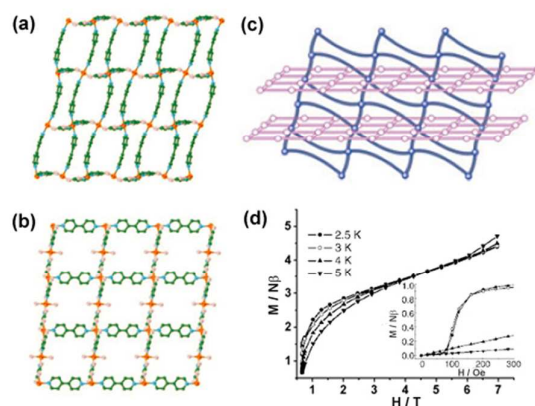
Figure 18 Views of the A-type (a) and B-type (b) sheets found in **35**. (c) A schematic representation of the orthogonal interpenetrated sheets (A-type sheet blue, B-type sheet pink). (d) Plots of the magnetization of **35** at 2–5 K with details at low fields of 0–300 Oe (Inset).

Although the 2D→3D parallel or inclined interpenetration of layers is not very unusual, the intertwining of different sheets is extremely rare coordination polymer chemistry. **35** present the first example of the inclined interpenetration of two types of sheets with different composites that have the same topology (4,4-net). The authors highlight the unique compact 3D extended network as features of a strong structural anisotropy from single-ion anisotropy to anisotropic chains, sheets and the final 3D structure. Both the 2.5 K isotherm and low-field magnetization presenting a small butterfly-shaped hysteresis exhibit spin canting and typical metamagnetism with a critical temperature T_c of 3.5 K and a critical field H_c of about 160 Oe.

Kitagawa *et al*. reported a novel 2-fold entangled porous framework, $[Zn_2(bdc)_2(dpNDI)]_n \cdot 4nDMF$ (**36**, dpNDI = N,N′-di(4-pyridyl)-1,4,5,8-naphthalenediimide).[64] One of the frameworks of **36** was intergrown at the central position of the void that was created by the other framework (Figure 19). Notably, both dpNDI and bdc moieties are unusually bent to enhance the preferential π–π stacking interactions with an inter framework distance of 3.35 Å along the two different directions of the Zn–bdc coordination modes. Therefore, two neighbouring dpNDI units exhibit almost perpendicular orientations. Although the frameworks are interpenetrated, there are still two types of void spaces: the characteristic slit between dpNDI and bdc (site A) and the remaining void space (site B). Two DMF molecules occupy both sites A and B. The desolvated crystals of **36** undergo a dynamic structural transformation to confine a class of

aromatic volatile organic compounds (VOCs). The framework without VOCs is not light emissive. However, an enhanced emission, which is detectable by the naked eye, was produced after VOCs was confined in the framework. The aromatic species benzene, toluene, xylene, anisole, and iodobenzene inclusion crystals were indicated as blue, cyan, green, yellow and red, respectively, which is resulted from host–guest interaction between the framework and guest molecules.
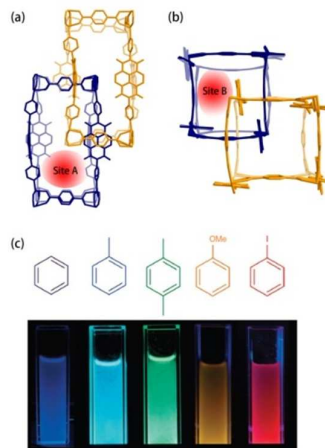
Figure 19 Views along the main axes of bdc (a) and dpNDI (b) in **36**, which exhibits slit-type pore of site A and site B. (c) Photos of the luminescence of crystal powders of **36**, suspended in different VOC liquids after excitation at 365 nm.

Driven by the vigorously pursuing of intricate and beautiful structures, interpenetration is an on-going objective being studied by numerous groups. Even so, the above examples showed that structural interpenetration is also closely associated with functional application of MOFs. Pores of small size and modified environment can be controlled by interpenetration, which could be beneficial to H_2 and CO_2 uptakes. Especially, the interaction of interpenetrated networks can lead to interesting dynamical behaviour and the guest-induced displacement of networks with respect to guest response. Due to the difference of coordination chemistry between ligands, mixed organic ligands strategy further brings abundant types of interpenetration. Especially, recent advance in this area have confirmed interpenetration can be manipulated by rational control of temperature, concentration, template and other factors. Combining mixed organic ligands strategy and interpenetration control makes interpenetrated mixed ligands MOFs new functional materials.

6 Perspectives

From above examples and other reports, there is no doubt that mixed organic ligands strategy is significant for the construction of MOFs. It provides fairly diverse selection of different organic ligands, which will promote the advances of MOFs from synthesis methodology, crystal engineering, and exploration of functions to future practical applications. The combination of different organic ligands and metals or clusters brings endless possibilities to generate MOFs with new structural topologies and functions. Rational knowledge of mixed organic ligands MOFs can be achieved by summarizing the preferred combination of different ligands, the influence factors that affect solubility of ligand, coordination tendency and compatibility of different ligands, crystal growth, and others. Then, design of mixed organic ligands system to realize target structures and properties are practicable. The persistent trial and subsequent findings and experience will contribute in turn to perfect our understanding about mixed organic ligands MOFs. Given that the never-ending choices of ligands and their diversiform combination, above virtuous circle will push the mixed organic ligands MOFs to a high level like the great success that

single ligand MOFs have reached. The sum of the physical properties of the mixed organic ligands and the inorganic components provide intriguing properties for a MOF. Especially, the possible synergistic play between the organic and inorganic part in the framework and also between the framework and guest inspire a new way of functionalization of MOFs. Recently, post-synthetic modification of MOFs has become a vibrant area of chemical research. Transmetalation of the SBU and post-synthetic modification/exchange of the organic linkers will be a prevalent technique for synthesizing MOFs that cannot be obtained de novo. When mixed organic ligands are applied, tandem and multiple post-synthetic modifications will be feasible to improve the performance of special properties or achieve a target functions. As highly developed materials, an area of great interest for MOFs that is worthy of further exploration is the introduce of nontoxic ligand like lactic acid, pyrimidine, porphyrin, nucleic acid, amino acid, and others to prepare environment friendly and biological compatible mixed organic ligands MOFs. In the future, biomedical application of MOFs, such as encapsulation and delivery of drugs, bioimaging, and biosensing would be of great potential to contribute to human health. Another promising area for mixed organic ligands MOFs is scaling them down to nanometer sizes. Nanoscale MOFs combine the merits of both MOFs and nanoparticles should have a bright future in a broader area.

Acknowledgment

List of abbreviations

1D = one dimensional
2D = two dimensional
3D = three dimensional
1,4-dimb = 1,4-di-(1-imidazolyl-methyl)-benzene
4,4′-bpy = 4,4′-bipyridine
5-NH$_2$-bdc = 5-aminoisophthalate
ad = adeninate
azpy = 4,4′-azopyridine
bpe = *trans*-1,2-bis(4-pyridyl)-ethylene
bpndc = benzophenone-4,4′-dicarboxylate
bphy = 1,2-bis(4-pyridyl)hydrazine
DMF = N,N′-dimethylformamide
DMA = N,N′-dimethylacetamide
DL-lac = DL-lactic acid
dpNI = N,N′-di(4-pyridyl)-1,4,5,8-naphthalenetetracarboxydiimide
dpNDI = N,N′-di(4-pyridyl)-1,4,5,8-naphthalenediimide
dpt = 3,6-Di-4-pyridyl-1,2,4,5-tetrazine
G = guest molecules
Hpybz = 4-(pyridin-4-yl)benzenecarboxylic acid
H$_2$bdc = 1,4-benzenedicarboxylic acid
H$_2$ca = D-(+)-camphoric acid
H$_2$hypa = hydroxy-phenyl-acetic acid
H$_2$muco = *trans*, *trans*-muconic acid

H₂ndc = naphthalene-2,6-dicarboxylate

H₂pico = 3-hydroxypicolinate

H₂pydc = 2,5-dicarboxypyridine

H₂pyrdc = pyridine-2,3-dicarboxylate

H₂pzdc = 2,3-pyrazinedicarboxylic acid

H₂suc = succinate

H₃tac = tricarballylate

H₃btc = 1,3,5-tris(4-carboxyphenyl)benzene

Hina = isonicotinate

L1 = 2,5-bis(2-hydroxyethoxy)-1,4-bis(4-pyridyl)benzene

ma = malate

MOF = metal-organic framework

pa = 3-(1*H*-benzimidazol-2-yl) propanoic carboxylate

SC-SC = Sing-crystal to sing-crystal

tcpp = 5,10,15,20-tetrakis(4-carboxyl)-21*H*,23*H*-porphine

VOCs = aromatic volatile organic compounds

Reference

[1] (a) H. Li, M. Eddaoudi, M. O'Keeffe and O. M. Yaghi, *Nature*, 1999, **402**, 276–279; (b) H. Furukawa, N. Ko, Y. B. Go, N. Aratani, S. B. Choi, E. Choi, A. O. Yazaydin, R. Q. Snurr, M. O'Keeffe, J. Kim and O. M. Yaghi, *Science*, 2010, **329**, 424–428.

[2] (a) N. L. Rosi, J. Eckert, M. Eddaoudi, D. T. Vodak, J. Kim, M. O'Keeffe and O. M. Yaghi, *Science*, 2003, **300**, 1127–1129; (b) L. Pan, B. Parker, X. Huang, D. H. Olson, J. Y. Lee and J. Li, *J. Am. Chem. Soc.*, 2006, **128**, 4180–4181; (c) C. Wu, A. Hu, L. Zhang and W. Lin, *J. Am. Chem. Soc.*, 2005, **127**, 8940–8941; (d) D. N. Dybtsev, A. L. Nuzhdin, H. Chun, K. P. Bryliakov, E. P. Talsi, V. P. Fedin and K. Kim, *Angew. Chem., Int. Ed.*, 2006, **45**, 916–920.

[3] (a) L. J. Murray, M. Dincă and J. R. Long, *Chem. Soc. Rev.*, 2009, **38**, 1294–1314; (b) Y. B. He, W. Zhou, G. D. Qian and B. L. Chen, *Chem. Soc. Rev.*, 2014, **43**, 5657–5678.

[4] J. R. Li, R. J. Kuppler and H.-C. Zhou, *Chem. Rev.*, 2012, **112**, 869–932.

[5] L. Q. Ma, C. Abney and W. B. Lin, *Chem. Soc. Rev.*, 2009, **38**, 1248–1256.

[6] Y. J. Cui, Y. F. Yue, G. D. Qian and B. L. Chen, *Chem. Rev.*, 2012, **112**, 1126–1162.

[7] (a) Z. C. Hu, B. J. Deibert and J. Li, *Chem. Soc. Rev.*, 2014, **43**, 5815–5840; (b) L. E. Kreno, K. Leong, O. K. Farha, M. Allendorf, R. P. V. Duyne and J. T. Hupp, *Chem. Rev.*, 2012, **112**, 1105–1125.

[8] (a) M. Kurmoo. *Chem. Soc. Rev.*, 2009, **38**, 1353–1379. (b) P. Ambenoit and J. R. Long, *Chem. Soc. Rev.*, 2011, **40**, 3249–3265.

[9] (a) Metal-organic frameworks themed issue, *Chem. Soc. Rev.*, 2014, **43**, 5415−6140; (b) Thematic issue of metal-organic frameworks, *Chem. Rev.*, 2012, **112**, 673−1268; (c) Metal-organic frameworks issue, *Chem. Soc. Rev.*, 2009, **38**, 1201−1508.

[10] J. P. Zhang, Y. B. Zhang, J. B. Lin and X. M. Chen, *Chem. Rev.*, 2012, **112**, 1001–1033.

[11] C. N. R. Rao, S. Natarajan and R. Vaidhyanathan, *Angew. Chem., Int. Ed.*, 2004, **43**, 1466–1496.

[12] M. Eddaoudi, J. Kim, N. L. Rosi, D. T. Vodak, J. Wachter, M. O'Keeffe and O. M. Yaghi, *Science*, 2002, **295**, 469–472.

[13] (a) S. S. Y. Chui, S. M. F. Lo, J. P. H. Charmant, A. G. Orpen and I. D. Williams, *Science*, 1999, **283**, 1148–1150; (b) J. F. Eubank, H. Mouttaki, A. J. Cairns, Y. Belmabkhout, L. Wojtas, R. Luebke, M. Alkordi and M. Eddaoudi, *J. Am. Chem. Soc.*, 2011, **133**, 14204–14207; (c) K. C. Stylianou, R. Heck, S. Y. Chong, J. Bacsa, J. T. A. Jones, Y. Z. Khimyak, D. Bradshaw and M. J. Rosseinsky, *J. Am. Chem. Soc.*, 2010, **132**, 4119–4130; (d) C. Y. Sun, S. X. Liu, D. D. Liang, K. Z. Shao, Y. H. Ren and Z. M. Su, *J. Am. Chem. Soc.* 2009, **131**, 1883–1888.

[14] (a) K. Otsubo, Y. Wakabayashi, J. Ohara, S. Yamamoto, H. Matsuzaki, H. Okamoto, K. Nitta, T. Uruga and H. Kitagawa, *Nature Mat.*, 2011, **10**, 291–295; (b) K. Li, L. Y. Zhang, C. Yan, S. C. Wei, M. Pan, L. Zhang and C. Y. Su, *J. Am. Chem. Soc.*, 2014, **136**, 4456–4459; (c) X. P. Zhou, Y. Wu and D. Li, *J. Am. Chem. Soc.*, 2010, **135,** 16062−16065; (d) Q. K. Liu, J. P. Ma and Y. B. Dong, *J. Am. Chem. Soc.*, 2010, **132**, 7005–7017; (e) P. Cui, Y. G. Ma, H. H. Li, B. Zhao, J. R. Li, P. Cheng, P. B. Balbuena and H. C. Zhou, *J. Am. Chem. Soc.*, 2012, **134**, 18892−18895; (f) Z. Z. Lu, R. Zhang, Y. Z. Li, Z. J. Guo and H. G. Zheng, *J. Am. Chem. Soc.*, 2011, **133**, 4172–4174; (g) S. M. Neville, G. J. Halder, K. W. Chapman, M. B. Duriska, P. D. Southon, J. D. Cashion, J. F. Létard, B. Moubaraki, K. S. Murray and C. J. Kepert, *J. Am. Chem. Soc.*, 2008, **130**, 2869–2876.

[15] (a) C. Kaes, A. Katz and M. W. Hosseini, *Chem. Rev.*, 2000, **100**, 3553–3590; (b) S. A. Barnett and N. R. Champness, *Coord. Chem. Rev.*, 2003, **246**, 145–168.

[16] (a) K. Harris, D. Fujita and M. Fujita, *Chem. Commun.*, 2013, **49**, 6703–6712; (b) Y. Inokuma, M. Kawano and M. Fujita, *Nature Chem.*, 2011, **3**, 349–358.

[17] (a) A. Y. Robin and K. M. Fromm, *Coord. Chem. Rev.*, 2006, **250**, 2127–2157; (b) M. Du, C. P. Li, M. Chen, Z.-W. Ge, X. Wang, L. Wang and C. S. Liu, *J. Am. Chem. Soc.*, 2014, **136**, 10906–10909; (c) R. Q. Zou, H. Sakurai and Q. Xu, *Angew. Chem., Int. Ed.*, 2006, **45**, 2542–2546.

[18] (a) B. H. Ye, M. L. Tong and X. M. Chen, *Coord. Chem. Rev.*, 2005, **249**, 545–565; (b) W. M. Xuan, C. C. Ye, M. N. Zhang, Z. J, Chen and Y. Cui, *Chem. Sci.*, 2013, **4**, 3154–3159; (c) P. D. Southon, D. J. Price, P. K. Nielsen, C. J. McKenzie and C. J. Kepert, *J. Am. Chem. Soc.*, 2011, **133**, 10885–10891; (d) B. Li, R. J. Wei, J. Tao, R. B. Huang, L. S. Zheng and Z. P. Zheng, *J. Am. Chem. Soc.*, 2010, **132**, 1558–1566; (e) M. Du, Z. H. Zhang, L. F. Tang, X. G. Wang, X. J. Zhao and S. R. Batten, *Chem. Eur. J.*, 2007, **13**, 2578–2586.

[19] (a) K. Otsubo, T. Haraguchi, O. Sakata, A. Fujiwara and H. Kitagawa, *J. Am. Chem. Soc.*, 2012, **134**, 9605–9608; (b) M. H. Mir, L. L. Koh, G. K. Tan and J. J. Vittal, *Angew. Chem., Int. Ed.*, 2010, **49**, 390–393.

[20] (a) Z. Yin, Q. X. Wang and M. H. Zeng, *J. Am. Chem. Soc.*, 2012, **134**, 4857–4863; (b) M. H. Zeng, Y. X. Tan, Y. P. He, Z. Yin, Q. Chen and M. Kurmoo, *Inorg. Chem.* 2013, **52**, 2353–2360.

[21] (a) Q. Chen, J. B. Lin, W. Xue, M. H. Zeng and X. M. Chen, *Inorg. Chem.*, 2011, **50**, 2321–2328; (b) Q. Chen, W. Xue, J.-B. Lin, R. B. Lin, M. H. Zeng and X. M. Chen, *Dalton Trans.*, 2012, **41**, 4199–4206; (c) Q. Chen, W. Xue, B. Y. Wang, M. H. Zeng and X. M. Chen, *CrystEngComm*, 2012, **14**, 2009–2014.

[22] (a) M. H. Zeng, X. L. Feng, W. X. Zhang and X. M. Chen, *Dalton Trans.*, 2006, 5294–5303; (b) Y. L. Zhou, M. C. Wu, M. H. Zeng and H. Liang, *Inorg. Chem.*, 2009, **48**, 10146–10150; (c) M. H. Zeng, Y. L. Zhou, M. C. Wu, H. L. Sun and Miao Du, *Inorg. Chem.*, 2010, **49**, 6436–6442.

[23] (a) M. H. Zeng, Q. X. Wang, Y. X. Tan, S. Hu, H. X. Zhao, L. S. Long and M. Kurmoo, *J. Am. Chem. Soc.*, 2010, **132**, 2561–2563. (b) M. H. Zeng, Z. Yin, Y. X. Tan, W. X. Zhang, Y. P. He and M. Kurmoo, *J. Am. Chem. Soc.*, 2014, **136**, 4680–4688.

[24] (a) Z. Q. Wang and Seth M. Cohen. *Chem. Soc. Rev.*, 2009, **38**, 1315–1329; (b) P. Deria, J. E. Mondloch, O. Karagiaridi, W. Bury, J. T. Hupp and O. K. Farha, *Chem. Soc. Rev.*, 2014, **43**, 5896–5912; (c) C. K. Brozek and M. Dinca, *Chem. Soc. Rev.*, 2014, **43**, 5456–5467.

[25] F. Sun, Z. Yin, Q. Q. Wang, D. Sun, M. H. Zeng and M. Kurmoo, *Angew. Chem., Int. Ed.*, 2013, **52**, 4538–4543.

[26] M. Du, C. P. Li, C. S. Liu and S. M. Fang, *Coord. Chem. Rev.*, 2013, **257**, 1282–1305.

[27] (a) M. Meilikhov, S. Furukawa, K. Hirai, R. A. Fischer and S. Kitagawa, *Angew. Chem., Int. Ed.*, 2013, **52**, 341–345; (b) T. Yamada and H. Kitagawa, *J. Am. Chem. Soc.*, 2009, **131**, 6312–6313; (c) Y. Y. Lin, Y. B. Zhang, J. P. Zhang and X. M. Chen, *Crystal Growth Des.*, 2008, **8**, 3673–3679; (d) Z. J. Lin, T. F. Liu, B. Xu, L. W. Han, Y. B. Huang and R. Cao, *CrystEngComm*, 2011, **13**, 3321–3324.

[28] M. H. Zeng, unpublished result.

[29] M. H. Zeng, unpublished result.

[30] M. H. Zeng, B. Wang, X. Y. Wang, W. X. Zhang, X. M. Chen and S. Gao, *Inorg. Chem.*, 2006, **45**, 7069–7076.

[31] Q. Chen, Y. L. Zhou and M. H. Zeng, *J. Mol. Struct.*, 2009, **932**, 55–60.

[32] M. H. Zeng, M. C. Wu, H. Liang, Y. L. Zhou, X. M. Chen and S. W. Ng, *Inorg. Chem.*, 2007, **46**, 7241–7243.

[33] M. H. Zeng, S. Gao and X. M. Chen, *Inorg. Chem. Commun.*, 2004, **7**, 864–867.

[34] J. Seo, R. Matsuda, H. Sakamoto, C. Bonneau and S. Kitagawa, *J. Am. Chem. Soc.*, 2009, **131**, 12792–12800.

[35] (a) W. Y. Gao, M. Chrzanowski and S. Q. Ma, *Chem. Soc. Rev.*, 2014, **43**, 5841–5866; (b) E.-Y. Choi, P. M. Barron, R. W. Novotny, H.-T. Son, C. Hu and W. Choe, *Inorg. Chem.*, 2009, **48**, 426–428.

[36] H. Chung, P. M. Barron, R. W. Novotny, H. T. Son, C. Hu and W. Choe, *Crystal Growth Des.*, 2009, **9**, 3327–3332.

[37] B. J. Burnett, P. M. Barron, C. Hu and W. Choe, *J. Am. Chem. Soc.*, 2011, **133**, 9984–9987.

[38] M. H. Zeng, X. L. Feng and X. M. Chen, *Dalton Trans.*, 2004, 2217–2223.

[39] M. H. Zeng, S. Hu, Q. Chen, G. Xie, Q. Shuai, S. L. Gao and L. Y. Tang. *Inorg. Chem.*, 2009, **48**, 7070–7079.

[40] P. Kanoo, G. Mostafa, R. Matsuda, S. Kitagawa and T. K. Maji, *Chem. Commun.*, 2011, **47**, 8106–8108.

[41] (a) D. Tanaka, K. Nakagawa, M. Higuchi, S. Horike, Y. Kubota, T. C. Kobayashi, M. Takata and S. Kitagawa, *Angew. Chem., Int. Ed.*, 2008, **47**, 3914–3918; (b) M. Du, X. J. Jiang and X. J. Zhao, *Inorg. Chem.*, 2007, **46**, 3984–3995.

[42] (a) H.-S. Choi and M. P. Suh, *Angew. Chem., Int. Ed.*, 2009, **48**, 6865–6869; (b) O. K. Farha, C. D. Malliakas, M.G. Kanatzidis and J. T. Hupp, *J. Am. Chem. Soc.*, 2010, **132**, 950–952.

[43] A. M. Shultz, O. K. Farha, J. T. Hupp and S. T. Nguyen, *J. Am. Chem. Soc.* 2009, **131**, 4204–4205.

[44] J. Zhang, Y. G. Yao and X. H. Bu, *Chem. Mater.*, **2007**, *19*, 5083–5089.

[45] (a) M. Kawano and M. Fujita, *Coord. Chem. Rev.*, 2007, **251**, 2592–2605; (b) A. Schneemann, V. Bon, I. Schwedler, I. Senkovska, S. Kaskel and R. A. Fischer., *Chem. Soc. Rev.*, 2014, **43**, 6062–6096; (c) J. P. Zhang, P. Q. Liao, H. L. Zhou, R. B. Lin and X. M. Chen, *Chem. Soc. Rev.*, 2014, **43**, 5789–5814; (d) Z. Yin and M. H. Zeng, *Sci. China Chem.*, 2011, **54**, 1371–1394; (e) X. D. Chen, X. H. Zhao, M. Chen and M. Du, *Chem. Eur. J.*, 2009, **15**, 12974–12977.

[46] D. N. Dybtsev, A. L. Nuzhdin, H. Chun, K. P. Bryliakov, E. P. Talsi, V. P. Fedin and K. Kim, *Angew. Chem., Int. Ed.*, 2005, **44**, 1–6.

[47] J. An, S. J. Geib and N. L. Rosi, *J. Am. Chem. Soc.*, 2009, **131**, 8376–8377.

[48] J. An and N. L. Rosi, *J. Am. Chem. Soc.*, 2010, **132**, 5578–5579.

[49] J. An, C. M. Shade, D. A. Chengelis-Czegan, S. Petoud and N. L. Rosi, *J. Am. Chem. Soc.*, 2011, **133**, 1220–1223.

[50] P. Horcajada, R. Gref, T. Baati, P. K. Allan, G. Maurin, P. Couvreur, G. Férey, R. E. Morris and C. Serre, *Chem. Rev.*, 2012, **112**, 782–835.

[51] W. X. Zhang, P. Q. Liao, R. B. Lin, Y. S. Wei, M. H. Zeng and X. M. Chen, *Coord. Chem. Rev.*, 2015, in press, doi: 10.1016/j.ccr.2014.12.009.

[52] A. C. Sudik, A. P. Cote, A. G. Wong-Foy, M. O'Keeffe and O. M. Yaghi, *Angew. Chem., Int. Ed.*, 2006, **45**, 2528–2533.

[53] J. R. Li and H. C. Zhou, *Angew. Chem., Int. Ed.*, 2009, **48**, 8465–8468.

[54] Y. B. Zhang, W. X. Zhang, F. Y. Feng, J. P. Zhang and X. M. Chen, *Angew. Chem. Int. Ed.*, 2009, **48**, 5287–5290.

[55] Y. B. Zhang, H. L. Zhou, R. B. Lin, C. Zhang, J. B. Lin, J. P. Zhang and X. M. Chen, *Nat. Commun.*, 2012, **3**, 642.

[56] X. Zhao, X. H. Bu, T. Wu, S. T. Zheng, L. Wang and P. Y. Feng, *Nat. Commun.*, 2013, **4**, 2344.

[57] Q. R. Fang, G. S. Zhu, Z. Jin, M. Xue, X. Wei, D. J. Wang and S. L. Qiu, *Angew. Chem., Int. Ed.*, 2006, **45**, 6126–6130.

[58] J. An, O. K. Farha, J. T. Hupp, E. Pohl, J. I. Yeh and N. L. Rosi, *Nat. Commun.*, 2012, **3**, 604.

[59] T. Li, M. T. Kozlowski, E. A. Doud, M. N. Blakely and N. L. Rosi, *J. Am. Chem. Soc.*, 2013, **135**, 11688–11691.

[60] X. L. Wang, C. Qin, S. X. Wu, K. Z. Shao, Y. Q. Lan, S. Wang, D. X. Zhu, Z. M. Su and E. B. Wang, *Angew. Chem., Int. Ed.*, 2009, **48**, 5291–5295.

[61] A. Schoedel, A. J. Cairns, Y. Belmabkhout, L. Wojtas, M. Mohamed, Z. J. Zhang, D. M. Proserpio, M. Eddaoudi and M. J. Zaworotko, *Angew. Chem., Int. Ed.*, 2013, **52**, 2902–2905.

[62] H. L. Jiang, T. Makal and H. C. Zhou, *Coord. Chem. Rev.*, 2013, **257**, 2232–2249.

[63] M. H. Zeng, W. X. Zhang, X. Z. Sun and X. M. Chen, *Angew. Chem., Int. Ed.*, 2005, **44**, 3079–3082.

[64] Y. Takashima, V. M. Martínez, S. H. Furukawa, M. Kondo, S. Shimomura, H. Uehara, M. Nakahama, K. Sugimoto and S. Kitagawa, *Nat. Commun.*, 2011, **2**, 168.

TOC
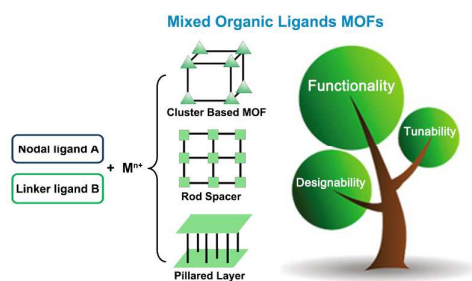
Mixed organic ligands strategy is significant for the rational construction of MOFs, furthermore for their functionality and tunability.